APPLICATION OF INTEGRATED GEOPHYSICAL TECHNIQUES TO

MAP GEOLOGICAL FEATURES FAVORABLE FOR THE LOCALIZATION OF GOLD

MINERALIZATION IN OKOTE, WEST GUJI ZONE, SOUTHERN ETHIOPIA

BY: GIRMA BAGAJO

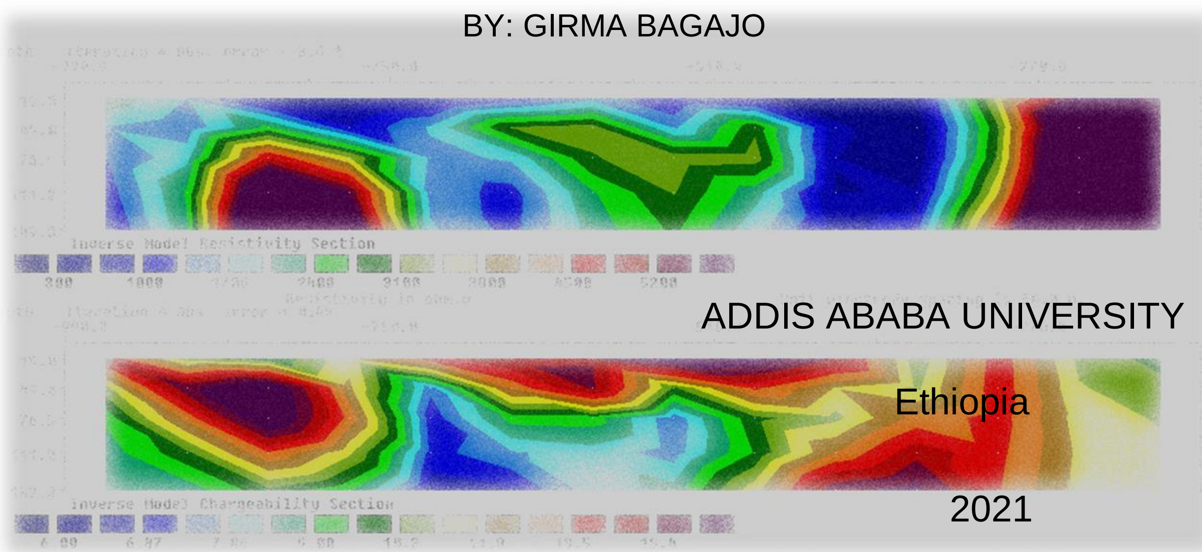

ADDIS ABABA UNIVERSITY

Ethiopia

2021

A THESIS SUBMITTED TO THE SCHOOL OF EARTH SCIENCES IN PARTIAL FULFILLMENT OF THE REQUIREMENT FOR THE DEGREE OF MASTER OF SCIENCE IN EXPLORATION GEOPHYSICS

ADVISOR: PROF.TILAHUN MAMMO

College of Natural and Computational Sciences

School of Earth Sciences

Applied geophysics stream

Thesis Approval Form

The research entitled as: Application of integrated geophysical techniques to map geological features favorable for the localization of gold mineralization in Okote, West Guji zone, Southern Ethiopia has been approved by the school graduate committee of School of Earth sciences for the partial fulfillment of the degree of Master of Science in Applied Geophysics.

Candidate: Girma Bagajo __________ ____________

Name **Signature** **Date**

Major Advisor: Professor Tilahun Mammo _________ ___________

Name **Signature** **Date**

Chairperson, School of Earth science: ________ __________ ___________

Name **Signature** **Date**

Chairperson, School Graduate committee: _________ ____________ ___________

Name **Signature** **Date**

ABSTRACT

Okote mineral prospect area is located in Hallo Kebele, Melka Soda district, West Guji zone of Oromia regional state in southern Ethiopia at about 610km south of Addis Ababa. The main purpose of this research project is to investigate characteristics and nature of gold mineralization in the area by applying integrated geophysical techniques.

Many researchers did research on the area and come up with different conclusions and recommendations. The Precambrian rock units containing a wide variety of sedimentary, volcanic and intrusive rocks which have been metamorphosed to varying degrees with one to six deformation phases, and different direction trending lineaments in the area were reported by different scholars.

This thesis research emphasizes the displaying of physical properties of the earth materials by using resistivity, induced polarization and magnetics techniques, which help to map the geologic features in relation to gold and associated mineralization's in the prospect area. In addition drill hole data and prior knowledge on geology of the area are integrated to discuss and interpret the plan maps, inverted section, enhanced magnetic anomaly maps and magnetic anomaly 2D modeling along the selected profiles.

The depth and lateral extension of the geological features are interpreted in detail based on the magnetic and chargeability anomalies. The high chargeability and high magnetic anomaly zones imply the presence of the sulfide mineralization's and ferromagnesian mineralization's respectively.

Interpretation is concentrated on searching promising sites for gold and associated mineralization s. The result is correlated with the geology of the area, and borehole data. Lastly recommendations will be made regarding the prospect area.

ACKNOWLEDGEMENT

First of all thanks to the merciful almighty God, which shows us his grace without asking its worth in our daily life circumstances.

I am indebted for their gratitude to Addis Ababa University, Wadera district water and energy resource development office, Ethiopia geological survey and Godu trading S.C. for their hand and perceptions through giving education opportunity and covering education fees, being sponsor and carrying work load in office on behalf of me, giving me favorable data (access me to secondary data) and giving me a research permission on licensed project site respectively.

My great appreciation and admiration is to my advisor professor Tilahun Mammo, who taught me, advises me kindly and shows me the ways wisely for the successfulness of this MSc thesis from beginning to the end of this work without saying they were tired.

I have a heartfelt gratitude and respect to Professor Tigistu Haile and to Dr. Abera Alemu for their advice, perception and on time response for what I asked for them during my research work.

I am grateful and lack the words to express the role of Mr. Wodesa Yachis, who financially support me while I was on education and at a field work. They initiatively encouraged me in order to follow my class and did my research works attentively and smoothly.

My heart felt admiration is to Mr. Addise Mokonnen (Chief Geologist at Godu) and Mr. Solomon Geda (PHD candidate) for their kindly support through accessing the data and precise background knowledge on Geology of Okote and Southern Ethiopia.

Finally, I intended to extend my thankful expressions to my father Bagajo Bulala and my mother Lomi Belako for their effort, moral support and harmless guidance in shortage and abundance. They are prime stakeholders for all my successfulness from beginning to the date of today.

Table of Contents

LIST OF FIGURES

LIST OF TABLES

ACRONYMS

nT……………………………………………………………nanotesla

ΩM---Ohm-meter

N---North

NW---Northwest

S---South

NE--Northeast

SW--Southwest

SE---Southeast

RTE--Reduce To Equatorial

RTP--Reduce To Pole

^{0}C---Degree centigrade

GPS--Global Position System

J_r--Remanent Magnetization

J_i--Induced Magnetization

IGRF---international Geomagnetic Reference Field

2D---Two-dimension

Msec---milliseconds

UTM--Universal Transverse Marcator

CGS--Centimeter-gram-second system

Am^{-1}--Ampere per meter

Msl--mean sea level

KM--Kilometer

m---meter

DH--drill-hole

EGS--Ethiopian geological survey

EIGS-- Ethiopian Institute of geological survey

MOME---ministry of mining and energy

NMIC---National Mining Corporation

IP--Induced polarization

Res---Resistivity

MB--Mozambique Belt

ANS--Arabian-Nubian shield

SI--Structural index

E---Electric field intensity

B_r---Radial component of magnetic field

B_θ--Tangential component of magnetic field

$B_\emptyset$--Longitudinal component of magnetic field

μ_r--Relative magnetic permeability

μ_O---Magnetic permeability of a vacuum

CHAPTER ONE

1. INTRODUCTION

1.1. LOCATION

Okote area is located in hallo kebele, melka soda woreda, west Guji zone of oromia regional state in southern Ethiopia at about 610km south of Addis Ababa, capital city of Ethiopia and located at South of Shakiso town of approximate distance of 100km. Geographically Okote prospect is located between $5^{0}06^{'}00^{"}$ to $5^{0}07^{'}20^{"}$ N latitude and $38^{0}46^{'}00^{"}$ to $38^{0}46^{'}45^{"}$ E longitude which is about $48km^{2}$ in areal extent, however proposed research is localized in to areal extent bounded by geographic coordinates between 38^{o} 46' 15"- 38^{o} 46' 40" E longitude and $5^{o}07'00"$ – 5^{o} 07'27"N latitude.

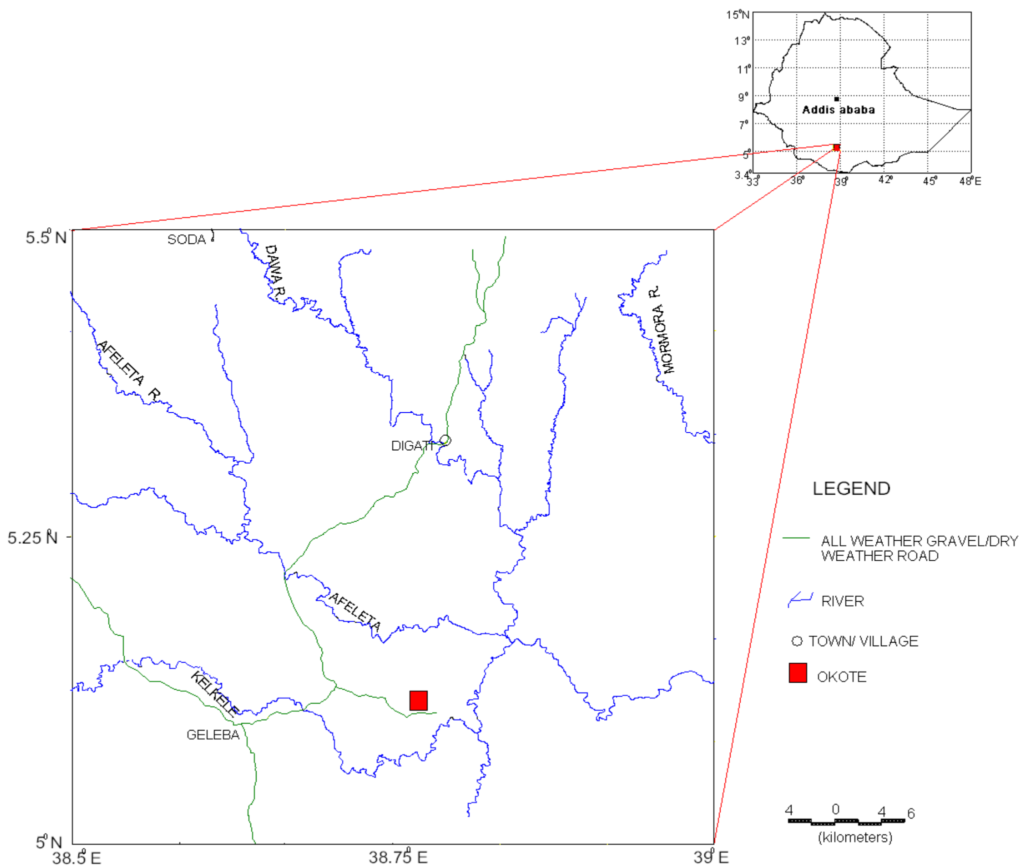

Figure 1. Location map of Okote area.

Figure 1.1. location map of okote area, *(Abu Wube,2005)*

1.2. ACCESSIBILITY

Project site is rugged and inaccessible for geophysical survey particularly for long cables instrumentation techniques. Gravel roads connect to the prospect area and exploration site reduce severity of in accessed terrain for transportation purpose. Several gravel roads and trenches have been constructed for the exploration purpose. In addition to this there are many trail ways that networking the study area to nearby densely populated Kebeles. Few temporary settlement currently covered the area in vicinity of project site along stream were serving society as shopping, restaurant center, grinding and panning service for artisana mining operations present in area.

1.3. PHYSIOGRAPHY AND CLIMATE

The study area is located in the southern part of the country in eastern Ethiopian plateau. The prospect site has hilly with numerous rugged terrain, steep ridges, valleys and deep gorges bounding the project area to the south, east and north-west. The project site itself ranges in elevation approximately from 1,300 to 1,500masl. The study area is not as such accessible for study especially for those geophysical surveys which does controlled by topographic variation between transmitter station and receiver station.

The project area is located in the semi-arid climate characterized by two rainy seasons peaking in May and October and this climatic regions, minimum and maximum temperatures remain approximately 10 ^{0}C and 25 ^{0}C respectively (Solomon Gada, 2019).

1.4. DRAINAGE PATTERN

The area of Okote is characterized by dendritic drainage pattern and by several drainage lines and rivers. Most of streams which show dendritic drainage pattern are ephemeral, but few of them flow throughout a year without cease its flow. Geleba, Dawa and Aflata rivers commonly known and good water potential rivers in the area which debouches to each other on east ward of the Okote project site, among which Aflata and Dawa rivers typically flow throughout a year without cease its flow, however it is understood that Aflata has rarely dry during very dry years (Solomon Geda, 2019).

1.5. VEGETATION COVERAGE, WILDLIFE

The project area is almost all sparsely vegetated with arid climate's vegetation of thin leaf and thorn worth plants and bushes but long and broad leaf trees are rarely available along the streams.

The area is home of several bird species, including Abyssinian Oriole and there is evidence of human pressure, resulting from habitation and artisanal mining activities that have a degrading effect on riparian habitats within the project area, however there is a low potential for medium and large mammals due to the pressure from human activities on habitats (Solomon Geda, 2019).

1.6. SOIL COVERAGE

The soil coverage is very thin in rugged topography and even lithologies are typically exposed to the surface whereas the soil coverage is somehow thick at the depositional landforms. The area is dominantly covered by thin red colored soil, hosting cobbles and boulders size milk quartz regolith.

1.7. OBJECTIVES

1.7.1. GENERAL OBJECTIVE

The main objective of the research is to apply integrated geophysical techniques that investigate the geological features favorable for the localization of gold occurrences in the Okote area, West Guji zone.

1.7.2. SPECIFIC OBJECTIVES

Specific objectives of the thesis research are, therefore:

- ✓ To map geological layers
- ✓ To detect and identify geological features, such as dyke, veins, intrusion, shear zones, folds,and litho-contacts as possible sites of gold and other associated mineralization.
- ✓ To identify host rocks for gold mineralization.
- ✓ To correlate geophysical result with geological and borehole data.

1.8. RESEARCH QUESTIONS

The following questions are answered in the research thesis:

- ➢ Is geologic setup and nature of geology favorable for gold mineralization?
- ➢ What are general preferred orientations of the geologic structures that are favorable for gold mineralization in Okote prospect area?
- ➢ What is the nature of gold mineralization?

  Is it associated with specific lithology?

  Is it structurally controlled?

1.9. RESEARCH PROBLEMS (STATEMENT OF PROBLEMS)

Borehole logs, earlier studied by EGS and MOME (2006) to correlate vertical lithological variations with the resistivity and chargeability do not show good correlations.

Again geologists and geophysicists did research on an area and did not recommended the extension (continuity) of anomaly prospect zones for further exploration in similar direction rather, geologists recommended north and south direction for further research whereas geophysicists recommended south west direction.

In order to solve these problems and to correct the mismatch between geophysical results and borehole data constrained geophysical inversion was done on the available resistivity and chargeability geophysical raw data, and an additional magnetic data were collected to clarify with what magnetic physical properties of the area behalf.

This research is focused on little modification of methodology of previous researches and interpreting the results by making further correlation of existing and newly collected data.

Therefore, in order to distinguish and identify clear location, orientation, depth, and other nature of mineral occurrences in the area it need intended researcher to do the research on the area. This research come up with good extra results which do not considered yet, and fill the gaps and contradicting idea in previous researches.

1.10. SIGNIFICANCE OF THE STUDY

The research describes about regional and local geology of an area as an introduction which is helpful to readers of the research to grasp the understanding of geological environment of study area. From the integrated geophysical methods applied on the area and analysis of secondary data the following critical results of the study were mentioned:

- ✓ The research solved previous mismatching of geophysical result and borehole data.
- ✓ The research solved previous mismatching of geophysical result and geological data.
- ✓ The research concisely answered the proposed basic research questions
- ✓ This research will be used for academic purpose
- ✓ The research will act as predictive research for the further researches
- ✓ The research will enhance researchers’ background knowledge

Generally, a research filled the gaps and contradiction in the previous researches.

1.11. LITERATURE REVIEWS

The regional geology of Adola gold field has been described by several researchers. The earliest published Study comes from (Billay et al., 1997) who makes a research on the geology of Laga Dambi gold deposit, and makes an implication for pan African gold exploration. (Solomon Gada., 2015) updated the geochemistry, alteration and genesis of granodiorite hosted gold mineralization in okote area.

In 1993/1994, an airborne geophysical survey consisting of electromagnetic, radiometric and magnetic methods was carried out in Borena region including Okote area. The aim of the survey was to provide information about geology and structure of the area. Geophysical investigations consisting of radiometric, IP/Res and magnetic methods were conducted in Okote area by Bulbul – Ageremariam mineral exploration project in 1988 and 1989.

Based on the agreement between GSE and NMiC, IP/Res survey was also carried out in Okote area in 1997. Even though, absolute coordinates of this area are not clearly defined, it is located south of the present area of investigation. IP/Res survey using the Gradient array delineated anomalous chargeability zone of about 25m width and 300m long corresponding to high apparent resistivity. Moreover, IP/Res survey using Dipole-Dipole array delineated high chargeability corresponding to high apparent resistivity having considerable depth and lateral extensions (Woldetinsae et al., 1997).

As the anomalies are open in the southwest of the surveyed Okote area, IP/res survey using the dipole-dipole array is suggested and detail IP/resistivity survey, preferably dipole-diploe section, is recommended on the zone of high resistivity and high chargeability association between 474750e and 474950e on the gradient array map (EIGS, MOME., 2006)

CHAPTER TWO

2.1. REGIONAL GEOLOGY

2.1.1. PRECAMBRIAN GEOLOGY OF ETHIOPIA

The Precambrian contains a wide variety of sedimentary, volcanic and intrusive rocks which have been metamorphosed to varying degrees (Asrat et al. 2001).

Precambrian basement of Ethiopia exposed in four geographically separate zones has been traditionally classified in to three stratigraphic units: the lower complex, the middle complex and the upper complex (Asrat et al. 2001).

There is confusion and little agreement in the application of the terms Pan-African Orogeny, Arabian-Nubian Shield (ANS) and Mozambique Belt (MB) to the Ethiopian basement (Asrat et al. 2001). Compilation and review of existing data on magmatic rocks indicate that the MB and ANS correspond to contemporaneous events of the Pan-African Orogeny, at least in Ethiopia, but with a difference in their tectonic evolution and degree of lateral denudation (Asrat et al. 2001).

The Precambrian geology of Ethiopia, although poorly understood, is of great interest because two major structures of Northeast Africa and Arabia meet in Ethiopia (Asrat et al. 2001).

The relation between the ANS and MB is far from clear but what emerges from previous data is as follows (table 2.1)

Feature	Arabian Nubian Shield (ANS)	Mozambique Belt (MB)
Dominant Rock Types	Mafic-ultramafic, juvenile (mantle derived) volcanic-plutonic associations and related metasediments	Gneisses and migmatites
Ophiolites	Abundant	Rare
Metamorphic Grade	Low (Green Schist facies)	Medium to High (Amphibolite -Granulite facies)
Assumed Mode of Formation	Lateral crustal growth (arc and terrane accretion ; or plate convergence (arc accretion and ocean closure) at a continental margin.	Himalayan type continental collision

Table 2.1. summary of the distinct features of ANS and MB, adopted from (Asrat et al. 2001)

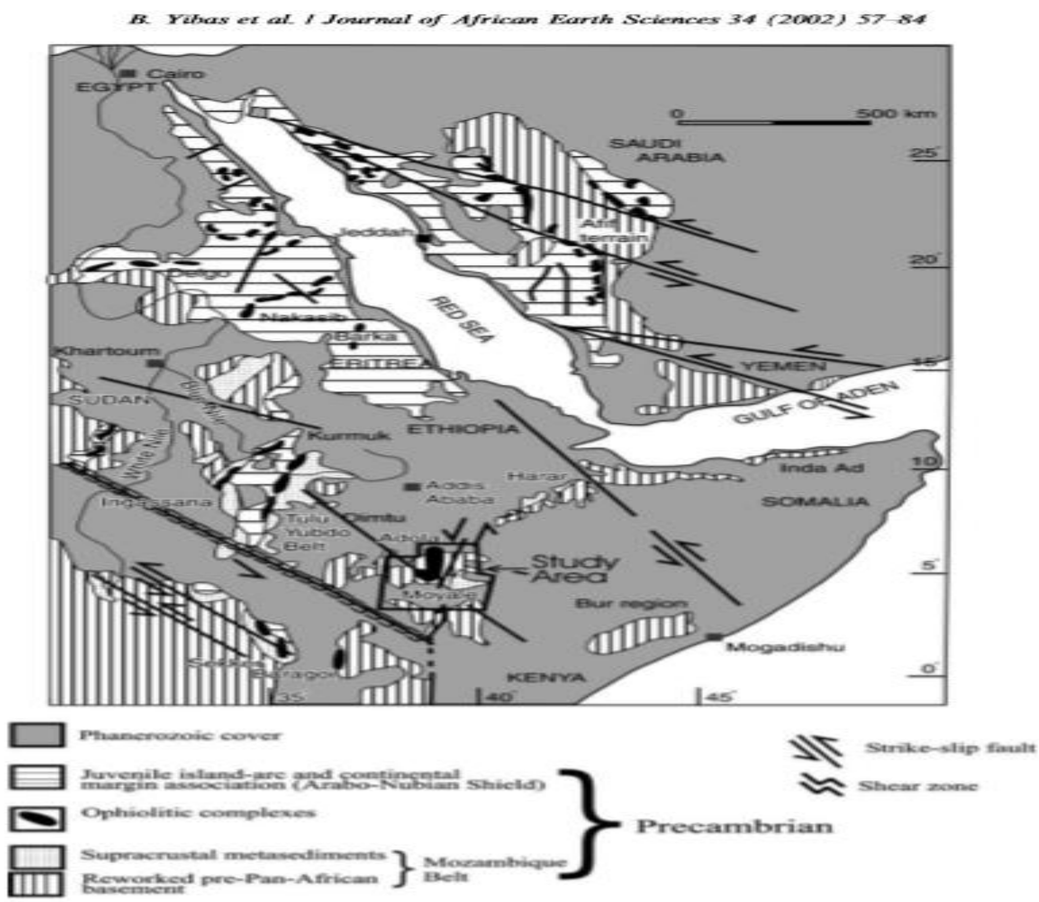

Figure 2.3. Geological map of northeastern Africa, modified after Worku and Schandelmeier (1996) and Shackleton (1997), showing the Precambrian of southern Ethiopia within the confines of the East African Orogen.

2.1.2. GEOLOGY AND TECTONOSTRATIGRAPHY OF SOUTH OF ETHIOPIA

The Precambrian geology of southern Ethiopia consists of two distinct lithotectonic terranes which show contrasting lithological association, internal structures and grade of metamorphism (Yibas et al., 2002): (1) the granite-gneiss terrane, consisting of high-grade para and orthogneisses and deformed and metamorphosed granitoids; and (2) the ophiolitic fold and thrust belts, consisting of low-grade, mafic–ultramafic and sedimentary assemblages. Major fault and/or shear zones displaying multiple deformation features (Yibas, 2002) separate these two terrane types. The Precambrian terrane of southern Ethiopia is overlain to the west by Cainozoic volcanics and sediments associated with the Main Ethiopian Rift System (Yibas, 2002).

In Adola, southern Ethiopia, mafic and ultramafic igneous rocks occur in narrow 4-10 km wide, north-south trending belts bounded by high-grade gneisses and migmatites (Solomon Geda, 2019).

2.1.2.1. GRANITE-GNEISS TERRANE

The granite-gneiss lithotectonic terrane has been subdivided into two sub-terranes (Burji–Moyale, Adola–Genale), and four complexes (Burji–Finchaa, Moyale–Sololo, Adola and Genale), based on the spatial associations of the rocks, internal structures, interrelationships of the various rock types and lithostructural similarity (Yibas, 2002).

2.1.2.2. OPHIOLITIC FOLD AND THRUST BELTS

Four mafic–ultramafic–sedimentary assemblages (each composed of varying proportions of mafic, ultramafic and sedimentary rocks) are recognised in the Precambrian of southern Ethiopia Yibas et.al (2002). These are the (1) Bulbul; (2) Kenticha; (3) Megado; and (4) Moyale–El Kur belts. The contacts of the ophiolitic fold and thrust belts with the adjacent granite-gneiss complexes are reactivated deformation zones, where evidence of both thrusting and strike-slip faulting could be found (Yibas et al. 2002).

2.1.3. PRECAMBRIAN GEOLOGICAL STRUCTURES

As a consequence of the E-W compression altectonic regime during orogenesis, a repetitive N-S oriented major antiforms and synforms, thrust and shear zones and related structures were generated (EIGS, 1998)

Ministry of Mines & Energy, and Ethiopian Institute of Geological Surveys, Regional Geology Department (1994) Studied Geology of Hagere mariam (Currently Bule Hora) and classified geological structures of an area in to six deformational events.

I. **First deformational phase (01):** The earliest deformational phase recognized is poorly represented due to the superimposition of later deformation and metamorphism. The earliest recognizable planar feature is defined by a well-developed layering in the high grade gneisses, formed by segregation of minerals. No major structure belonging to this deformational phase has been distinguished. Folds and lineations belonging to this phase of deformation are very scarce.

II. **Second deformational phase (D2**): Structures belonging to this deformational phase are well developed. The planar structures, folds and lineations of this phase are restricted to the high grade gneisses. This phase is regarded as the second most prominent event after D1 in the **high grade rocks,** controlling the outcrop pattern and producing N-S structural trends.

III. **Third deformational phase (D3):** Structures grouped under this deformational event are mainly widespread large to small shear zones and associated asymmetric folds. These shear zones generally trend NNW, NNE and N-S, with steep dips to east or west.

IV. **Fourth deformational phase (04):** Structures of this phase are similar to 02 structures and are seen mostly in the Adola low grade belt. The structural trend is north-south, with steep dips to east or west. This is the first tectonic event to affect the rocks of the Adola low grade belt.

V. **Fifth deformational phase (05):** Generally north-south trending shear zones and associated asymmetric folds deforming 04 structures are grouped in the fifth deformational event. Such features are abundant in the low grade rocks of the Adola belt. The shear zones are dominantly sinistral strike-slip.

VI. **Sixth deformational phase (D6)**: This deformation is weak and is represented mainly by mesoscopic, symmetrical folds with small amplitudes with east-west trending axial planes and gently to steeply plunging fold axes. Some E-W folds of this phase are macroscopic. Brittle and brittle-ductile faults up to 30 m in length cutting all earlier deformational features were noted and faults are dominantly dextral strike slip and of northerly trend.

LINEAMENT

As Mentioned in Ministry of Mines And Energy, And Ethiopian Institute of Geological Surveys, Regional Geology Department (1994) compilation on geology of Hagere Mariam (currently Bule Hora) lineaments in the area described and categorized as follows:

"The lineaments are mostly fractures (both joints and faults), but include stream segments, topographic depressions, ridges and various linear tonal variations on air photographs. Lineaments are best developed in the western and eastern parts of the map area. In the central part, where the topography is subdued, they are less conspicuous.

- **N-S trending lineaments (0°-010**°): are the dominant ones in the area. Such lineaments up to 20 km long are common, and are particularly abundant in the eastern and western parts of the map sheet of Hagere Mariam (Bule Hora).
- **NW trending lineaments (300°-330**°): are the second most common group, being especially widespread in the central and western parts of the area.
- **NNE trending lineaments (010°-030°):** are also widespread and generally display lengths varying from 5 to 10 km. A few prominent NE trending lineaments are present in the eastern part of the map area."

PHASES OF METAMORPHISM

Based on field investigations, structural correlation and petrographic study of various rock units in the Bule Hora, at least three metamorphic episodes affected both the high and the low grade rocks and three distinct prograde metamorphic events and a later retrograde overprint were recognized by Ministry of Mines & Energy, and Ethiopian Institute of Geological Surveys (1994), they explained three phases of metamorphism in an area as mentioned below:

The earliest recognizable thermal event (H1) in the area is represented by large scale migmatization, pegmatization and granitization. These features are well displayed in some of the high grade stratified gneisses.

The second metamorphic event (M2) is displayed by the stratified gneissic rocks in the region and the early intrusive unit. This event is regional in character as it is represented by widespread metamorphic mineral assemblages.

Third metamorphic event (M3): Following the M2 regional metamorphism a lower grade metamorphic event (M3) took place. This event appears to have been generally restricted to the Adola low grade belt and indicate upper greenschist facies metamorphism.

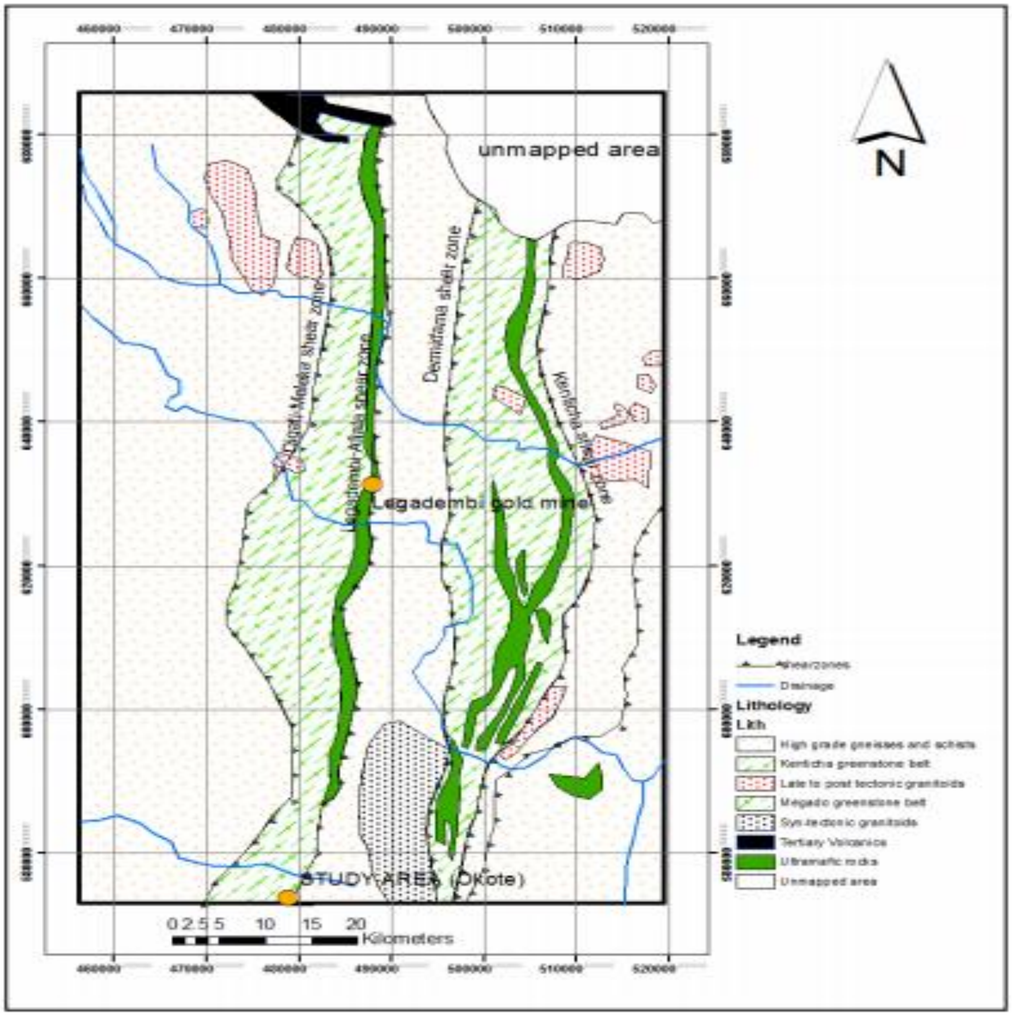

Litho-structural domains of Adola belt (Worku and Schandelmeier, 1996)

Figure 2.5. litho-structural domain of Adola belt adopted from (Solomon Geda, 2019)

2.1.4. REGIONAL DISTRIBUTION OF METALLIC MINERAL RESOURCES

The earliest exploration of a metallic mineral resource (gold) started in the late 1890s at Tulu Kami in the Kata area of western Ethiopia and most exploration activities had been conducted until the mid-1960s, in various regions, in a generally unorganized manner; however an exceptions are the significant placer gold deposits, which were discovered during World War II in the Adola region by Italian geologists (Mesresha et al. 2000). Systematic exploration and mining development so far undertaken in Ethiopia indicates the low-grade metavolcano-sedimentary sequences as the main repositories of precious, base, rare, and ferrous-ferroalloy metals (Mesresha, Selassie and relmold, 2000)

Three low-grade metavolcano-sedimentary domains and associated intrusive of the Arabo-Nubian Shield occur in three of southern, western and northern Ethiopia (mesresha et al. 2000)

- The fIrst can be subdivided into the Adola and Kenticha belts comprising the primary gold of Lega Dembi, Sakaro, Wollena, Kumudu, Megado-Serdo, Dawa-Digati, Moyale, and Ababa River; the columbo-tantalite of Kenticha and Meleka; and the Adola nickel deposit.
- The second domain can be subdivided into four belts, namely the Dul-Nazila, Menghi-Gizen, FakushoOda and Akobo-Yubdo-Baruda belts. These belts contain the primary gold of Oda-Godere, Chamo (Akobo), Yubdo platinum; base metals of Azali-Akendeyu, Abetselo and Kata; Fakusho molybdenite; and the iron deposits of bikilal, Chago, Gordana and Koree.
- The third major domain occurs in the Tigray region extending north to the neighboring state of Eritrea. This mafic-ultramafic terranes domain comprises the primary gold occurrences.

2.2. LOCAL GEOLOGY

2.2.1. GEOLOGY OF OKOTE

Okote prospect area is thoroughly covered by felsic and mafic metavolcanics often mylonitized at their contacts (Solomon Geda, 2019). The felsic rocks are repeatedly observed intruding the mafic rocks, and Metadiorite, Metagabbro, Amphibolite, Chlorite Amphibole schist, Chlorite/Carbonate-Chlorite schist and Talc schist are the intermediate-ultramafic sequences exposed on the prospect (Solomon Geda, 2019). Metagabro cut by three main shear zones that host gold mineralization (Debele j. deksisa and Christian koebel 2004). Metagabro has gradational contacts with meta-volcanics and meta-ultramafic rocks, but sharp contact with metagranodiorite (Debele j.

deksisa and Christian koebel 2004). Apilitic dyke is commonly intruding the mafic metavolcanics of the prospect (Solomon Geda, 2019). Euhedral pyrite and magenetite crystals are observed at several places, particularly in the tremolite-actinolite-talc schist (Solomon Geda, 2019).

The Okote gold mineralization is an example of such an extremely complicated system including, with at least two styles of gold mineralization including vein type and granodiorite hosted disseminated types (Solomon Geda, 2019). Metagranodiorite mineralization is characterized by disseminated sulphides and sulphides are undeformed and not aligned both down dip and along strike instead they are randomly dispersed in the rock unit (Solomon Geda, 2019).

Four main types of quartz veins are known in Okote prospect (Solomon Geda, 2019). The first three are concordant, while the last one is discordant to the regional foliation and the east-west running discordant quartz vein is characterized by glassy textured and barren with respect to gold (Solomon Geda, 2019). This might indicate that the E-W discordant quartz vein originated by a post deformational event cross-cutting the earlier mineralization (Solomon Geda, 2019). The concordant glassy textured quartz vein trends towards NNW-SSE and NNE-SSW along the shear zone which is characterized by sulphidation and tourmalinization (Solomon Geda, 2019). .

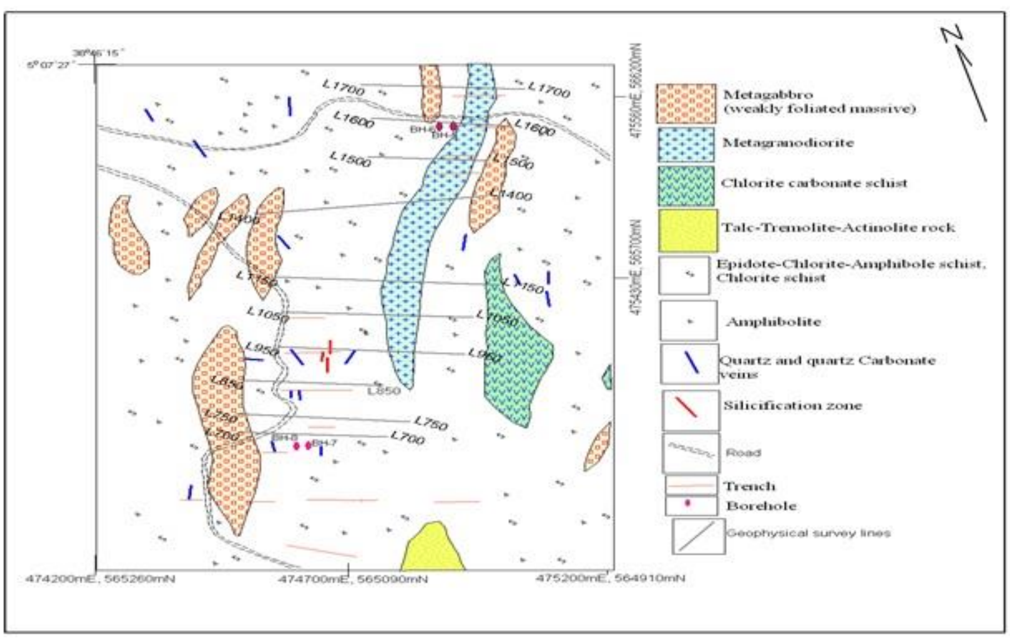

Figure 2.6. Geological map of Okote adopted from EGS and MOME (2006)

2.2.2. SHEARING, ALTERATION AND GOLD MINERALIZATION

The two major structures are N-S striking ductile shear zone, younger NW-SE trending brittle structure and minor structure strike E-W, and Structure and alteration zoning have been observed within N_S trending shear zone (Debele j. deksisa and Christian koebel, 2004).

Four types of alteration zones exist in the area, carbonatization, feldsphatization, tourmalinization and sericitization, and Zonings of alteration in typical magmatic hydrothermal alteration are common features of Okote granodiorite mineralization (Solomon Geda, 2019). The fractures are commonly filled by quartz and quartz carbonate veinlets (Debele j. deksisa and Christian koebel, 2004).

Mineralization in the okote is restricted to the anastomosing system of narrow high strain, N-S trending ductile shear zones and the ores minerals are dessimated in the quartz veins and in the wall rock alteration are dominantly pyrite, minor magnetite, chalcopyrite, pyrrhotite, ilmenite, chalcocite, covelite, native gold, galena, melonite and wolframite (Debele j. deksisa and Christian koebel, 2004).

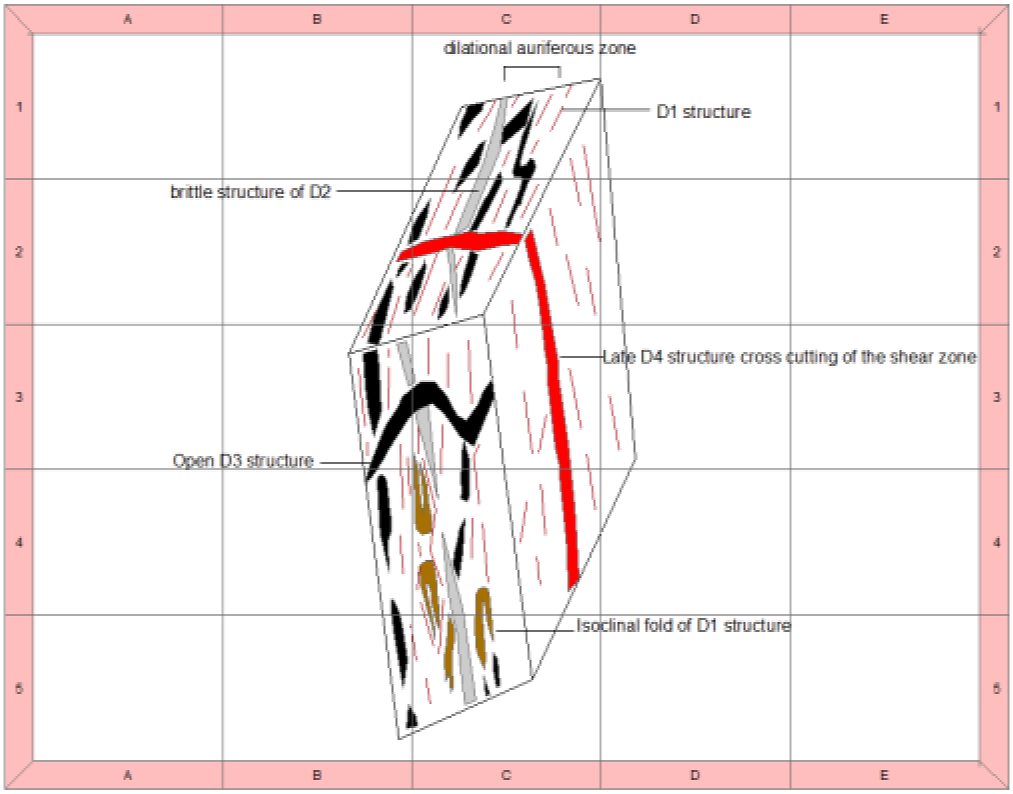

Figure 2.7.Schematic model showing deformational events of Okote (D1, D2, D3 and D4) with their cross-cutting relationships (Solomon Geda, 2019)

CHAPTER THREE

3. THEORY AND FUNDAMENTAL CONCEPTS

3.1. BASIC RESISTIVITY METHOD THEORY

The resistivity (geologic resistivity) method is a geophysical techniques used to investigate the vertical and horizontal discontinuities in resistivity of the subsurface formation (Abera Alemu, 2020).

The purpose of electrical surveys is to determine the subsurface resistivity distribution by making measurements on the ground surface. From these measurements, the true resistivity of the subsurface can be estimated and the ground resistivity is related to various geological parameters such as the mineral and fluid content, porosity and degree of water saturation in the rock (loke 2004).

Electrical resistivity surveys have been used for many decades in hydrogeological, mining and geotechnical investigations and more recently, it has been used for environmental surveys (loke 2004).

The fundamental physical law used in resistivity surveys is Ohm's Law that governs the flow of current in the ground (loke 2004) and the equation for Ohm's Law in vector form for current flow in a continuous medium is given by

$$J = \sigma E \ldots\ldots 1.1$$

Where σ is the conductivity of the medium, J is the current density and E is the electric field intensity. In practice, what is measured is the electric field potential and we note that in geophysical surveys the medium resistivity ρ, which is equals to the reciprocal of the conductivity (ρ=1/σ), is more commonly used (loke 2004). The relationship between the electric potential and the field intensity is given by

$$E = -\Delta \mathrm{V} \ldots\ldots\ldots 1.2$$

Combining equations (1.1) and (1.2), we get

$$J = -\sigma \Delta V \ldots\ldots. 1.3$$

In this case, the current flows radially away from the source, and the potential varies inversely with distance from the current source, while equipotential surfaces have a hemisphere shape, and the current flow is perpendicular to the equipotential surface (loke 2004).The potential in this case is given by

$V = {}^{\rho l}/_{2\pi r}$, Where r is the distance of a point in the medium (including the ground surface) from the electrode. In practice, all resistivity surveys use at least two current electrodes, a positive current and a negative current source. The potential values have a symmetrical pattern about the vertical place at the mid-point between the two electrodes (loke 2004). The potential value in the medium from such a pair is given by

$$V = \frac{\rho l}{2\pi}\left(\frac{1}{r_{c1}} - \frac{1}{r_{c2}}\right),$$

where r_{C1} and r_{C2} are distances of the point from the first and second current electrodes. In practically all surveys, the potential difference between two points (normally on the ground surface) is measured (loke 2004). The potential difference is then given by:

$$\Delta V = \frac{\rho l}{2\pi}\left(\frac{1}{r_{c1P1}} - \frac{1}{r_{c2P1}} - \frac{1}{r_{c1p2}} + \frac{1}{r_{c2p2}}\right),$$

The above equation gives the potential that would be measured over a homogenous half space with a 4 electrodes array mean while the actual field surveys are invariably conducted over an inhomogeneous medium where the subsurface resistivity has a 3-D distribution (loke 2004). The resistivity measurements are still made by injecting current into the ground through the two current electrodes (C1 and C2), and measuring the resulting voltage difference at two potential electrodes (P1 and P2). From the current (I) and potential (∆V) values, an apparent resistivity (ρa) value is calculated (loke 2004).

$$\rho a = k\left(\frac{\Delta V}{I}\right)$$

$$k = \frac{2\pi}{\left(\frac{1}{r_{c1P1}} - \frac{1}{r_{c2P1}} - \frac{1}{r_{c1p2}} + \frac{1}{r_{c2p2}}\right),}$$

K is a geometric factor that depends on the arrangement of the four electrodes. Resistivity measuring instruments normally give a resistance value, $R = {}^{\Delta V}/_{I}$ so in practice the apparent resistivity value is calculated by $\rho a = kR$

The calculated resistivity value is not the true resistivity of the subsurface, but an “apparent” value that is the resistivity of a homogeneous ground that will give the same resistance value for the same electrode arrangement (loke 2004). The relationship between the “apparent” resistivity and the “true” resistivity is a complex relationship, and to determine the true subsurface resistivity from the apparent resistivity values is the “inversion” problem (loke 2004).

3.1.1. ELECTRODE ARRAYS

Many different array geometries have been used, and the more important ones are shown in Figure (), together with their formulas used to calculate the apparent resistivity. There are often differences of convenience between arrays, depending on the type of survey, as well as some differences in depth of penetration and resolution; these are only touched upon (Mussett and Khan, 2000).

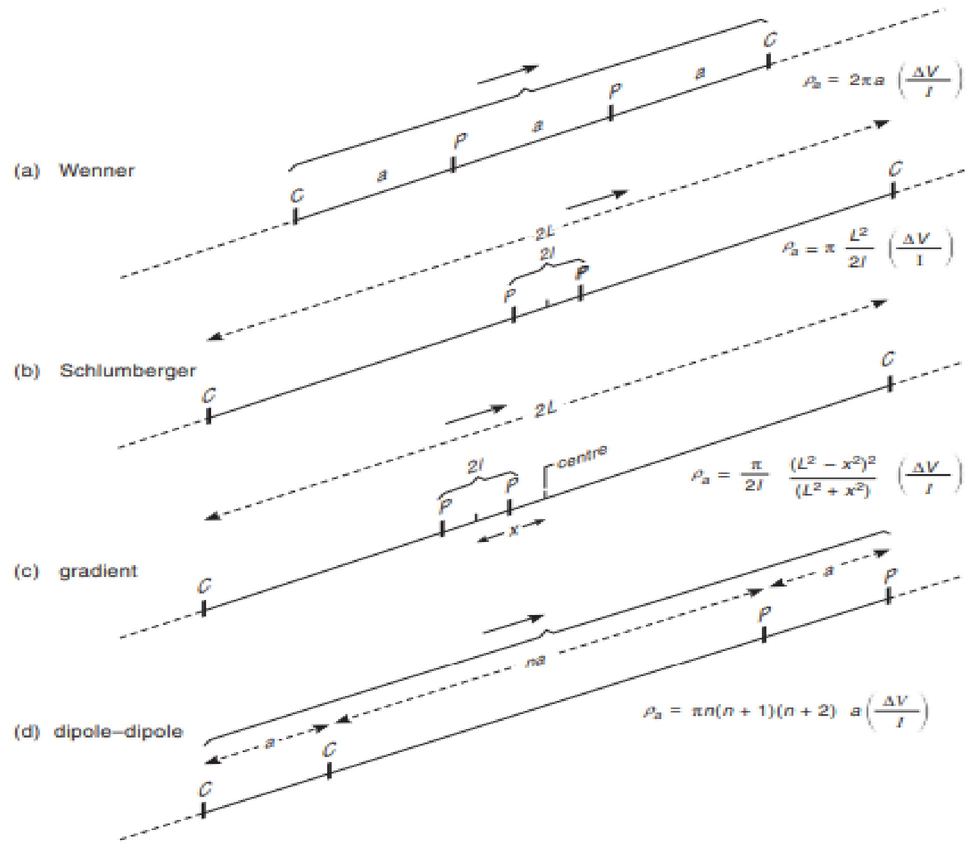

Figure 3.1. Varies resistivity arrays adopted from (Mussett and Khan, 2000).

3.1.2. ELECTRICAL PROPERTIES OF EARTH MATERIALS

Electric current flows in earth materials at shallow depths through two main methods. They are electronic conduction and electrolytic conduction (loke, 2004). In electronic conduction, the current flow is via free electrons, such as in metals. In electrolytic conduction, the current flow is via the movement of ions in groundwater and an electronic conduction is important when conductive minerals are present, such metal sulfides and graphite in mineral surveys.

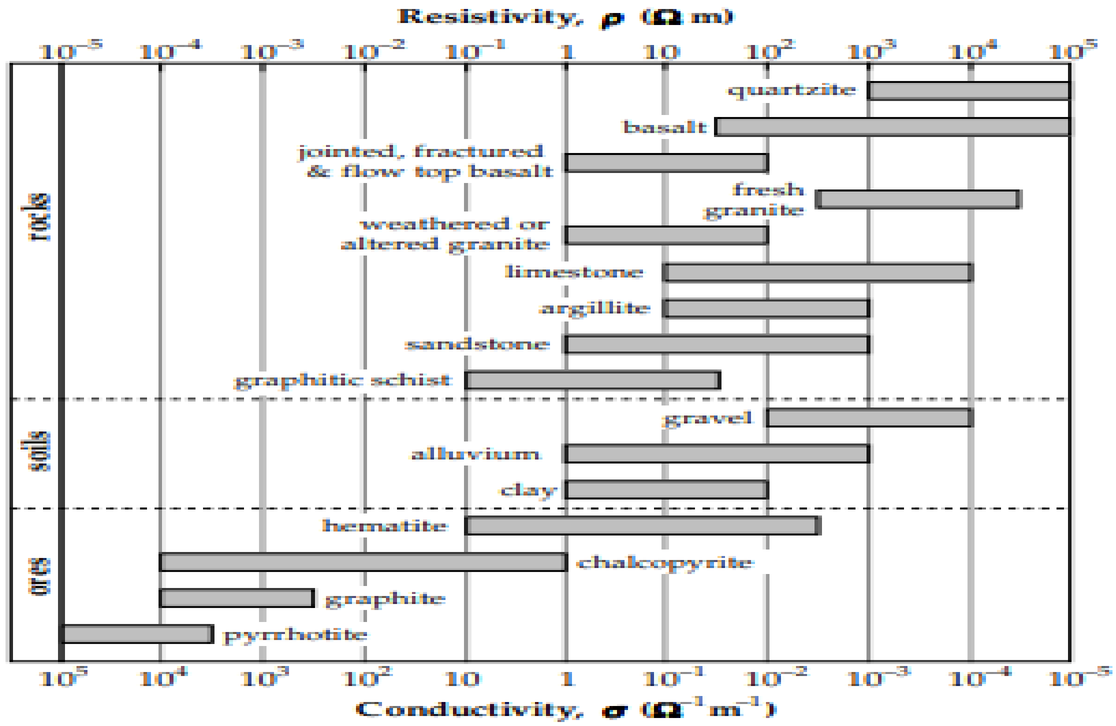

Table 3.1. Ranges of electrical resistivity for some common rocks, soils and ores (lowrie, 2007)

3.1.3. RESISTIVITY MODELING

3.1.3.1. VERTICAL ELECTRICAL SOUNDING

A two-layer situation is encountered often in electrical prospecting, for example when a conducting overburden overlies a resistive basement and two-layer cases were interpreted with the aid of characteristic curves and these theoretical curves, calculated for a particular four-electrode array, take into account the change in depth penetration when current lines cross the boundary to a layer with different resistivity and at a boundary the current lines behave like optical or seismic rays, and are guided by similar laws of reflection and refraction (lowrie, 2007).

$$\frac{tan\theta_1}{tan\theta_2} = \frac{\rho_2}{\rho_1} \text{ is low of refraction.}$$

The resistivity contrast is expressed by k-factor

$$k = \frac{\rho_2 - \rho_1}{\rho_2 + \rho_1}, -1 \le k \le 1 \text{ as } 0 \le \frac{\rho_2}{\rho_1}$$

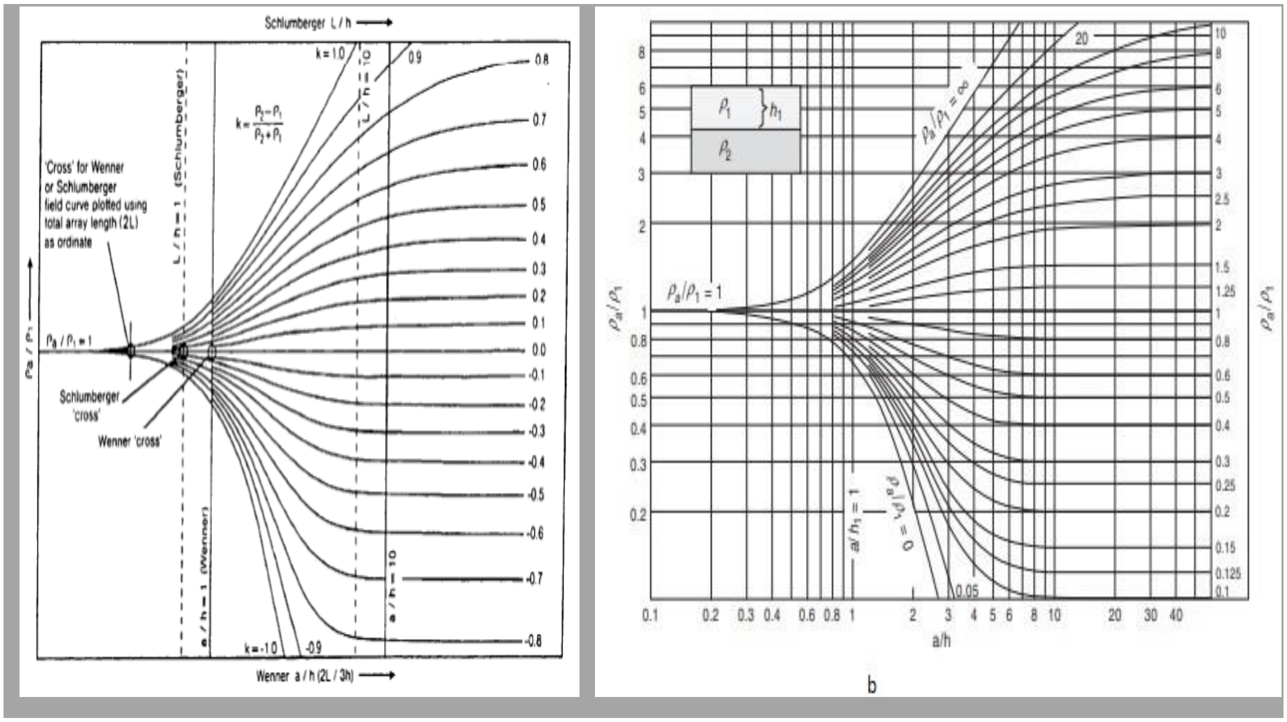

Figure 3.2. Characteristic curves of apparent resistivity for a two-layer structure using the Wenner array and schlunberger array (lowrie, 2007) and (b) Wenner array master curves for two layers(Mussett and Khan, 2000).

The apparent resistivity curve for a three-layer structure generally has one of four typical shapes, determined by the vertical sequence of resistivity in the layers (lowrie, 2007). The type K curve rises to a maximum then decreases, indicating that the intermediate layer has higher resistivity than the top and bottom layers. The type H curve shows the opposite effect; it falls to a minimum then increases again due to an intermediate layer that is a better conductor than the top and bottom layers. The type **A** curve may show some changes in gradient but the apparent resistivity generally increases continuously with increasing electrode separation, indicating that the true resistivities increase with depth from layer to layer. The type Q curve exhibits the opposite effect; it decreases continuously along with a progressive decrease of resistivity with depth.

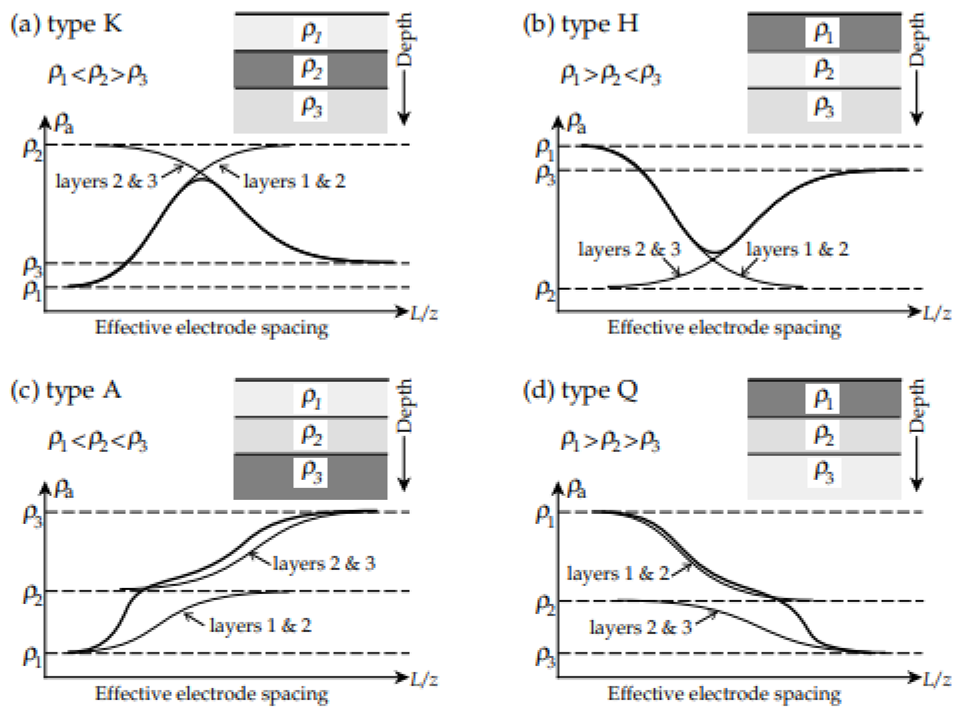

Figure 3.3. the four common shapes of apparent resistivity curves for a layered structure consisting of three horizontal layers (source: lowrie, 2007).

3.2. INDUCED POLARIZATION

The induced polarization method makes use of the capacitive action of the subsurface to locate zones where conductive minerals are disseminated within their host rocks (Abera alemu, 2020).

When using a standard four-electrode resistivity spread in a DC mode, if the current is abruptly switched off, the voltage between the potential electrodes does not drop to zero immediately. After a large initial decrease the voltage suffers a gradual decay and can take many seconds to reach a zero value. A similar phenomenon is observed as the current is switched on. After an initial sudden voltage increase, the voltage increases gradually over a discrete time interval to a steady-state value. The ground thus acts as a capacitor and stores electrical charge, that is, becomes electrically polarized (Mussett and Khan, 2000).

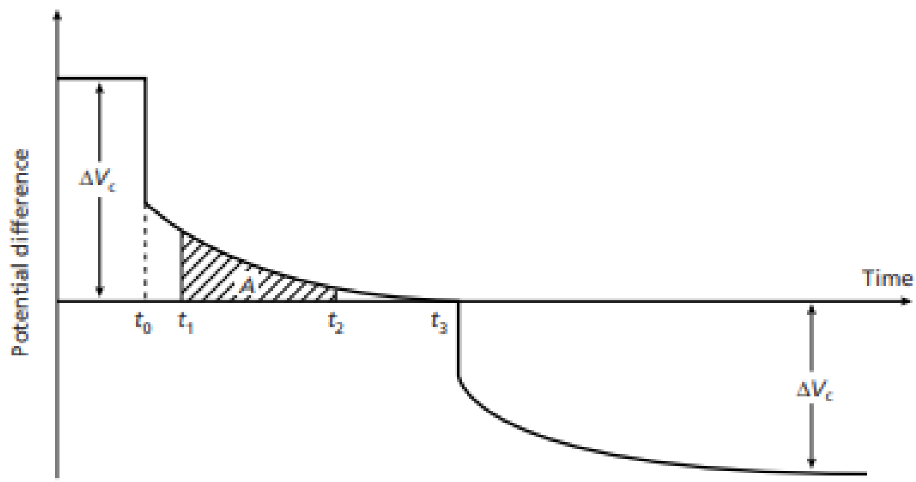

Figure 3.4. the phenomenon of induced polarization. At time t_0 the current is switched off and the measured potential difference, after an initial large drop from the steady-state valueΔVc, decays gradually to zero. A similar sequence occurs when the current is switched on at time t_3. **A** represents the area under the decay curve for the time increment t 1-t 2 ((Mussett and Khan, 2000).

IP surveys are perhaps the most useful of all geophysical methods in mineral exploration, being the only ones responsive to low-grade disseminated mineralization. There are two main mechanisms of rock polarization and three main ways in which polarization effects can be measured (loke, 2004). In theory the results obtained by the different techniques are equivalent but there are practical differences.

i. **Membrane polarization:** The surfaces of clays and some other platey or fibrous minerals are negatively charged and cause membrane polarization in rocks with small pore spaces.
ii. **Electrode polarization:** This electrode polarization occurs not merely at artificial electrodes but wherever grains of electronically conducting minerals are in contact with the groundwater. Strong anomalies are also usually produced by massive sulphide mineralization, because of surrounding disseminated haloes.

3.2.1. INDUCED POLARIZATION DATA

The methods used to display IP data vary with the array and profiles or contour maps are used for gradient arrays, while dipole–dipole data are almost always presented as pseudo-sections (loke, 2004).

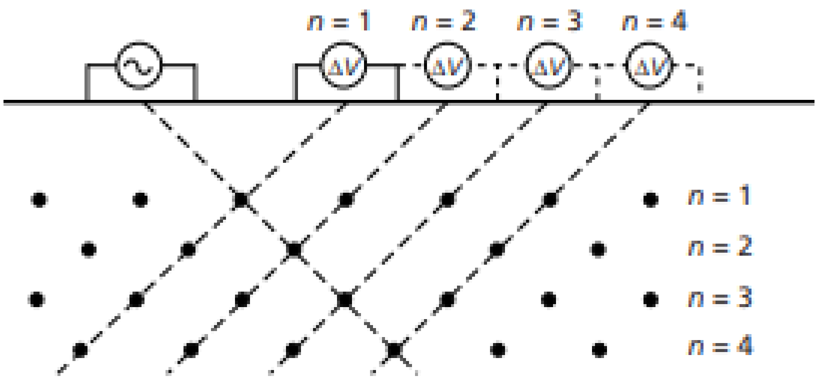

Figure 3.5. The presentation of dipole-dipole IP results on a pseudo section. n represents the relative spacing between the current and potential electrode pairs (Mussett and Khan, 2000).

3.2.2. NEGATIVE INDUCED POLARIZATIONS AND MASKING

Negative IP effects can be caused by power or telephone cables or, as shown, by signal contribution sections or by lateral in-homogeneities and also layering can also produce negative values, and can conceal deeper sources, most readily if both the surface and target layers are more conductive than the rocks in between (loke, 2004).

3.3. BASIC MAGNETIC THEORY

3.3.1. ORIGIN OF MAGNETIC FIELD

The electrostatics field is the only force field that exists around a charge at rest, however if the charge begins to move, another kind of force field that can also exert forces on magnetic substances is immediately introduced. This force field which is introduced by the charge in motion (current) is known as a magnetic field (Abera Alemu, 2020).

Within the vicinity of a bar magnet a magnetic fluxis developed which flows from one end of the magnet to the other (the poles of the magnet). This flux can be mapped by a small compass needle suspended within it. Similarly, a magnet aligns in the flux of the Earth's magnetic field (Marescot, 2002).

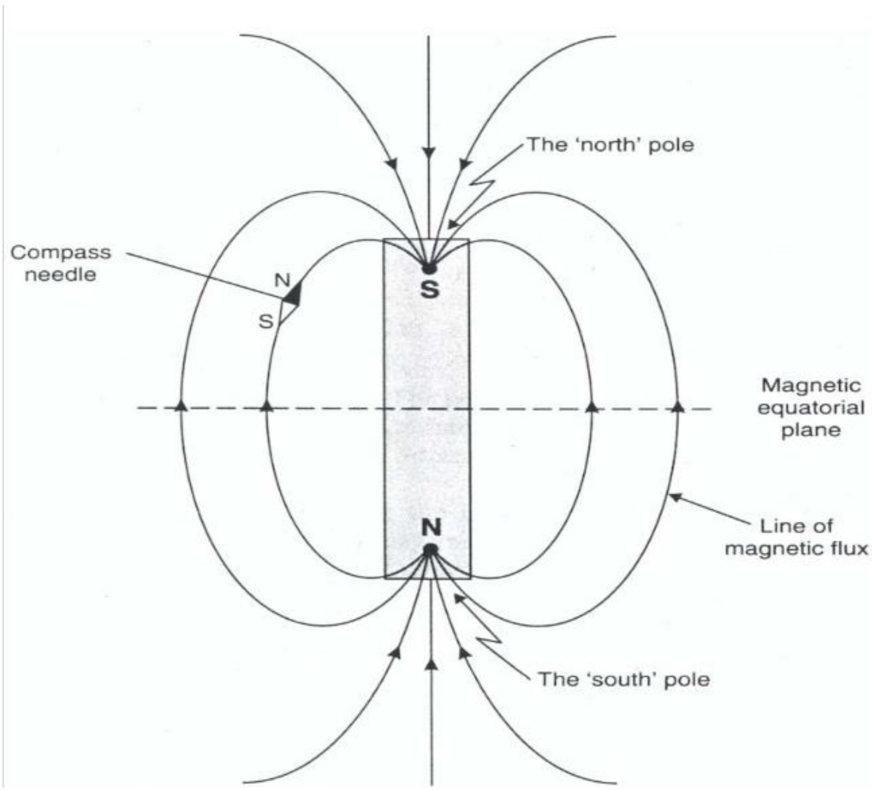

Figure 3.6. Flow of magnetic flux adopted from (Marescot, 2002).

3.3.2. FORCES BETWEEN TWO MAGNETIC POLES

The forces between two magnetic poles of strengths m1 and m2 (Marescot, 2002)

$$\vec{F} = \frac{\mu_O M1M2}{4\pi\mu_r r^2}\vec{r}$$

Figure 3.7. forces between magnetic poles adopted from magnetic surveying (Marescot, 2002).

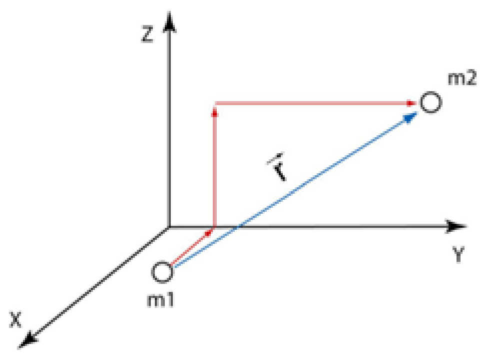

$\mu_O = 4\pi x 10^{-2} Vs/\, AM$, This is magnetic permeability of a vacuum.

$$\mu_r = \frac{\mu}{\mu_O}$$

Where: μ_r=relative permeability

μ=medium permeability

3.3.3. MAGNETIC MOMENT

The magnetic moment is the vector joining the two poles–m and +m (at distance r apart) (Marescot, 2002).

$\vec{M} = \frac{M}{\vec{r}}$, in AM^2

3.3.4. EARTH'S MAGNETIC FIELD AND MAGNETIC POTENTIAL

The variation of magnetic field with altitude, latitude and longitude are dominated by the vertical and horizontal variation of the dipole field and at any point the dipole field has a radial component B_r and tangential component B_θ which can be obtained by differentiating the dipole potential W with respect to r and θ respectively (Abera Alemu, 2020).

The radial component of magnetic field is given as:

$$B_r = -\frac{\partial W}{\partial r} = -\frac{\partial}{\partial r}\left(\frac{1}{4\pi\mu}\frac{M}{r^2}cos\theta\right) = 2\frac{M}{4\pi\mu r^3}cos\theta$$

Tangential component B_θ $(0 \leq \theta \leq 180)$ of the earth magnetic field is given as:

$$B_\theta = -\frac{1}{r}\frac{\partial W}{\partial \theta} = -\frac{1}{r}\frac{\partial}{\partial \theta}\left(\frac{1}{4\pi\mu}\frac{M}{r^2}cos\theta\right) = -\frac{M}{4\pi\mu r^3}sin\theta$$

The longitudinal component $B_\emptyset$ $(0 \leq \emptyset \leq 360)$

$\boldsymbol{B_\emptyset} = -\frac{\mathbf{1}}{\boldsymbol{rsin\theta}}\frac{\boldsymbol{\partial W}}{\boldsymbol{\partial \emptyset}} = -\frac{\mathbf{1}}{\boldsymbol{rsin\theta}}\frac{\boldsymbol{\partial}}{\boldsymbol{\partial \emptyset}}\left(\frac{\mathbf{1}}{\boldsymbol{4\pi\mu}}\frac{\boldsymbol{M}}{\boldsymbol{r^2}}\boldsymbol{cos\theta}\right) = 0$, magnetic potential does not vary with $\emptyset$.

3.3.5. ROCK MAGNETIZATION

when magnetizable material such as iron is immersed in an externally magnetic field B the material will acquire its its own magnetism known as induced magnetization J_i usually oriented in direction parallel to the direction of external field (Abera Alemu,2020). In the absence of an external magnetization B-field, there is still a measurable amount of magnetization preserved by certain rock types due to permanently magnetized particles of the rocks. This type of magnetization is known as remnant magnetization denoted by J_r (Abera Alemu, 2020).

$J= J_i+J_r$

Where, J is rock magnetization, J_i is induced magnetization and J_r is remnant magnetization

$J_i=kB$, where k is magnetic susceptibility, B is magnetic field

The intensity of induced magnetizationis defined as the magnetic moment per unit volume of material (Marescot, 2002).

$$\overrightarrow{Ji} = \frac{\overrightarrow{M}}{V}$$

The magnetic susceptibility k is dimensionless and determines the degree of magnetization of materials.

$$\boldsymbol{K} = \frac{\overrightarrow{\boldsymbol{Ji}}}{\overrightarrow{\boldsymbol{H}}}$$

H simply describes how B is modified by the magnetic polarization (or magnetization M).

The susceptibility, k, is very small for most natural materials, and may be either negative (diamagnetism) or positive (paramagnetism) and the fields produced by diamagnetic and paramagnetic materials are usually considered to be too small to affect survey magnetometers, but modern high-sensitivity magnetometers are creating exceptions to this rule (Milsom, 2003).

Most observed magnetic anomalies are due to the small number of ferro- or ferri-magnetic substances in which the molecular magnets are held parallel by intermolecular exchange forces (milsom, 2003).

The susceptablitlites of various rocks and minerals	
Material	Susceptibility x 10^{-3} (SI)
Air	about 0
Quartz	-0.01
Rock Salt	-0.01
Calcite	-0.001 - 0.01
Sphalerite	0.4
Pyrite	0.05 - 5
Hematite	0.5 - 35
Illmenite	300 - 3500
Magnetite	1200 - 19,200
Limestones	0 - 3
Sandstones	0 - 20
Shales	0.01 - 15
Schist	0.3 - 3
Gneiss	0.1 - 25
Slate	0 - 35
Granite	0 - 50
Gabbro	1 - 90
Basalt	0.2 - 175
Peridotite	90 - 200

Table (3) magnetic susceptibility of the common rocks and minerals adopted from **(**Emerson and the Australian Society Of Exploration Geophysicists, 1980)

3.3.6. GEOMAGNETIC ELEMENTS

A vector that describes the magnetic field strength and direction from a given position can be broken into its components as the follows (Lillie, 1999)

$\vec{F}$= total magnetic field

$\overrightarrow{Fh}$=horizontal component of total field vector

$\overrightarrow{Fn}$=north component of horizontal vector

$\overrightarrow{Fe}$=east component of horizontal vector

$\overrightarrow{Fv}$= vertical component of total vector i= angle of magnetic inclination

δ=angle of magnetic declination

The magnitude (F) of the total magnetic field vector (total field intensity) is

$$F = \sqrt{(Fh)^2 + (Fv)^2}$$

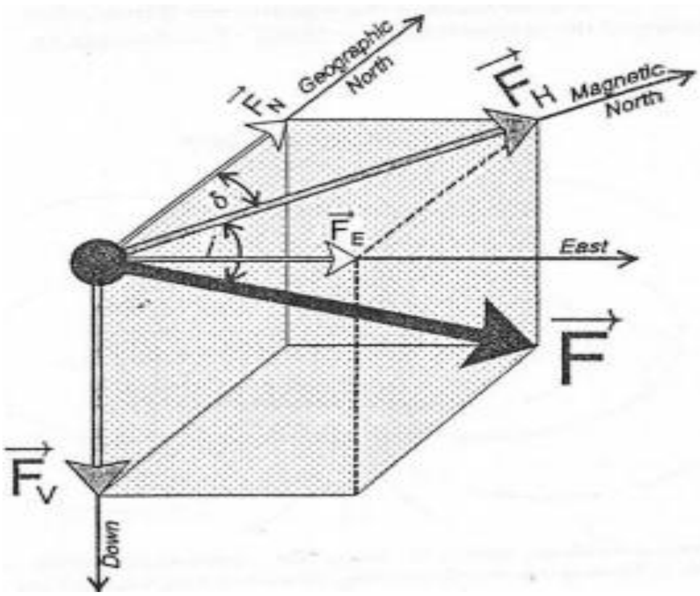

Figure 3.8. Elements of magnetic field adopted from whole earth geophysics textbook (Lillie, 1999)

CHAPTER FOUR

4. METHODOLOGY AND GEOPHYSICAL DATA

4.1. METHODOLOGY

This MSc thesis compilation is derived from integration of both primary and secondary data. Secondary data is collected by EGS and MOME in 2006. The electrical data was collected data by IPR-10A and IPR-12 receivers, TSQ-3 transmitter and 8HP Briggs and Stratton motor generator. The Dipole-Dipole array was conducted using IPR-12 and the Gradient array data was produced by using the IPR-10A receiver.

Both IP and resistivity data were collected by dipole-dipole electrode arrangement and central gradient array. Dipole-dipole array was conducted on eight lines with one to six n-Spacing and 60m unit electrode spacing, whereas central gradient array data was collected from two lines (950N and 1050N). Every measurement was conducted on each line by shifting 10m electrode positions.

Magnetic survey was conducted on ten survey lines along which resistivity and chargeability data were collected from and the data were acquired in a systematic sampling technique by using earth magnetometer, Garmin GPS and Brunton compass.

Oasis montaj geosoft and Res2dinv softwares were used to process both primary and secondary data to plot resistivity and chargeability plan map, resistivity and chargeability inverted section and magnetic anomalies maps and 2D magnetic anomaly modeling. Resistivity and chargeability plan map, magnetic maps and 2D magnetic anomaly model were plotted by using oasis montaj geosoft, whereas resistivity and chargeability inverted sections were plotted by Res2dinv software.

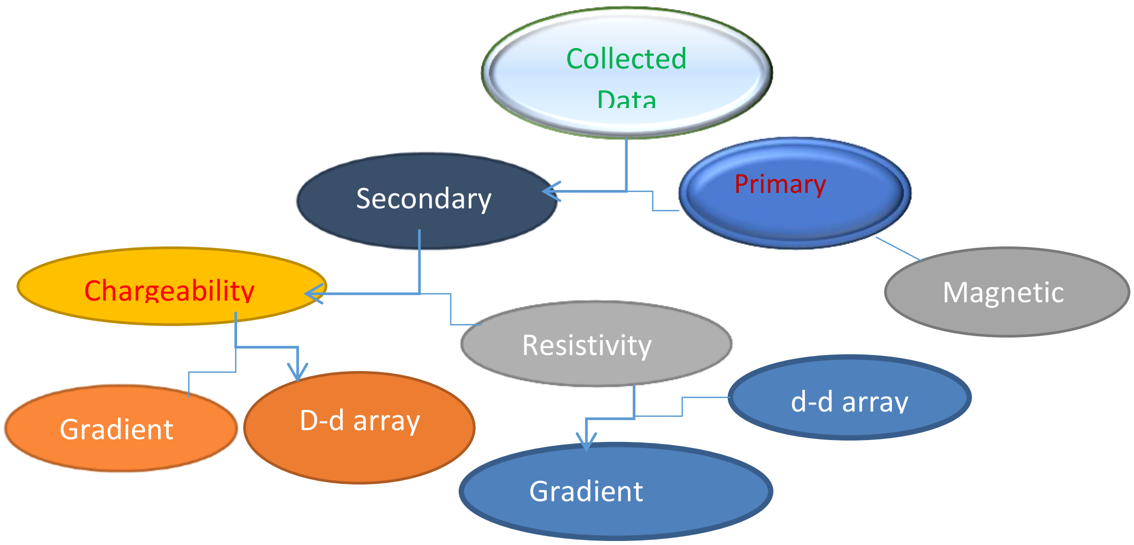

Figure 4.1. Flow chart of the methodology

4.2. FIELD PROCEDURES AND DATA PROCESSING

4.2.1. FIELD PROCEDURES

A) ELECTRICAL DATA COLLECTION PROCEDURES

The Dipole-Dipole array was conducted along eight survey lines, namely 700N, 750N, 850N 1150N, 1400N, 1500N, 1600N and 1700N. Measurements were made with “n" spacing of 1 to 6. Apparent resistivity and chargeability of individual transients were measured every 10m station interval. The sketch below shows the Dipole-Dipole array.

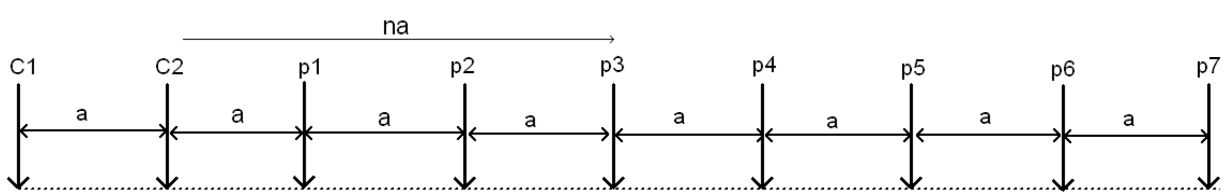

Figure 4.2. Sketch of dipole-dipole array

n =1- 6

a = 60m

C1, C2 = Current electrodes

P1, P2… = Potential electrodes

The Gradient array was conducted along two lines (950N and 1050N) using potential electrodes separation of 20 m and sampling interval of 10 m. The current electrodes C1 and C2 were fixed at 1250W and 150E (i.e. C1C2=1400 m) and readings were taken between stations 750W and 300W. Below is shown a schematic representation of the field configuration.

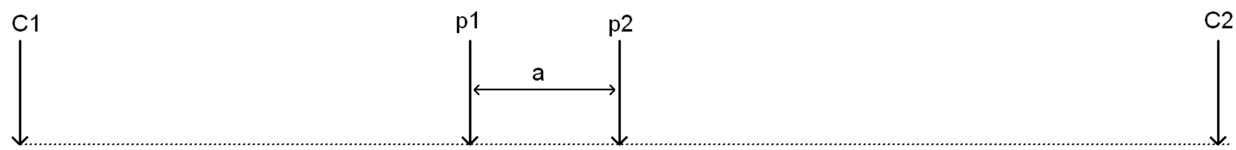

Figure 4.3.Sketch (2) gradient arrey

The field data acquired was dumped to computer after each survey and arranged in the Geosoft format. The Geosoft Oasis Montaj data processing and mapping software was used to plot the data and to inspect any error encountered during data acquisition.

B) MAGNETIC DATA COLLECTION PROCEDURES

Magnetic data is collected along the same line from which resistivity and induced polarization survey was conducted contemporaneously. It is collected by systematic sampling technique from ten survey lines using earth magnetometer instrument. Acquired data were filtered for noise (diurnal variation) and processed by oasis montaj geosoft to be interpreted and correlated with maps of resistivity and chargeability data.

4.2.2. DATA PROCESSING

4.2.2.1 RESISTIVITY AND CHARGEABILITY DATA PROCESSING

A) PLAN MAP

Data of n-space ranges from n-1 to n-6 infer different geological material at various depths of investigation. The owners of resistivity and chargeability data were processed and presented 1, 3, & 5 n-spacing data. However in thesis work n-spacing raw data (n1, n2, n4 and n6) were arranged according to oasis montaj file format to be processed and presented accordingly. Compare and contrast of these plan maps according to their respective depth were clearly defined in the next section of interpretation.

The central gradient array data acquired from line 950N and line 1050N was arranged in the Geosoft format. The Geosoft Oasis Montaj data processing and mapping software was used to plot maps.

B) INVERTED SECTIONS

Resistivity and chargeability data were arranged according to res2dinv software file format, indix format particularly dipole-dipole indix format was saved in notepad before start processing and the data was inverted using RES2DINV software programmes to be displayed as 2-D inverted maps. Both resistivity and chargeability data of eight lines were presented as inverted pseudo sections. Generally 16 inverted maps of both resistivity and chargeability data were discussed in the following interpretation section.

4.2.2.2. MAGNETIC DATA PROCESSING

Total magnetic field data collected from the field are corrected for diurnal variations by using Microsoft- excel and then the data are arranged for geosoft computer program software file format and imported. After importing: converting and defining coordinates, calculating IGRF, correcting data for IGRF, filtering, applying channel math calculation, gridding and mapping of desired magnetic anomalies data base was took place accordingly. Residual magnetic field anomaly was presented in the magnetic anomaly maps and magnetic anomaly models based on selected profile line.

CHAPTER FIVE

5. INTERPRETATION OF THE RESULTS

5.1. INTERPRETATION OF MAGNETIC FIELD MAPS

A) TOTAL MAGNETIC FIELD

Earth total magnetic field is composed of external field (B_{ext}), dipole field (B_D) and rock magnetism (B_{rm}). Rock magnetism is emphasis on the magnetic field generated from shallow earth materials and it is very useful for exploration of resources hidden from direct observation. However magnetic field varied due to temporal variations (diurnal variation, magnetic storm and secular variation) which lead in to erroneous interpretation. In order to get accurate results of rock magnetism (residual anomaly), careful measurements and reduction applied to total magnetic field is mandatory. Correction to the variation (noise) and filter applied to corrected magnetic anomaly are presented and interpreted consequently as the follows.

B) TOTAL MAGNETIC FIELD ANOMALY

Total magnetic field anomaly is an observed magnetic field anomaly resulted from total magnetic field corrected from diurnal variation and international geomagnetic reference field (IGRF). The corrections are take place by adding or subtracting of correction value from total magnetic field for diurnal correction and subtracting IGRF for reduction of dipole magnetic field.

Total magnetic field anomaly map (figure 5.1) is diurnally and IGRF corrected map for which no reduction to equatorial is applied on. It depicts low magnetic anomaly at south, east, north and northwest portion of study area. Southwest, central and some eastern zones of survey area are covered by distributions of high observed magnetic field anomaly.

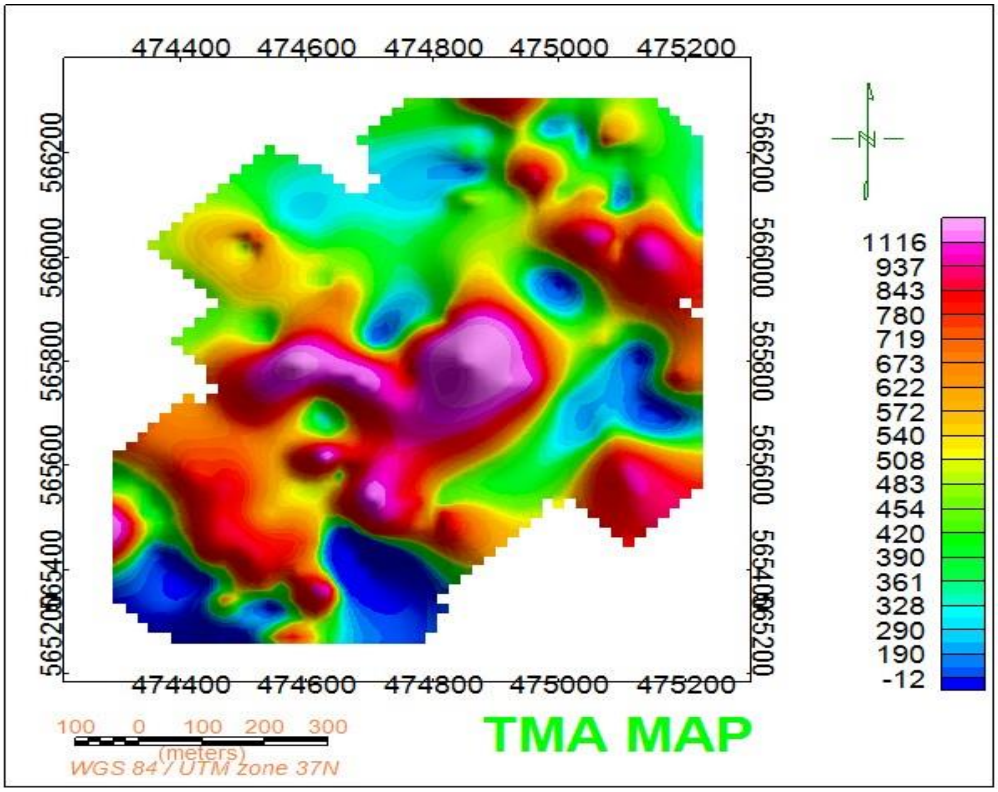

Figure 5.1. Total magnetic field anomaly map

C) RESIDUAL MAGNETIC FIELD ANOMALY

Residual magnetic anomaly is obtained when regional magnetic field anomaly is removed from total magnetic field anomaly. It is magnetic field of the rock magnetism that arises from shallow earth materials of which the effect of long wave length is attenuated and that of short wave length is enhanced.

In this case (figure 5.2) magnetic field anomaly generated from the depth less than 250m is enhanced while magnetic field emanated beneath 250m depth is suppressed (attenuated). Okote is located at equatorial area and magnetic fields collected from equatorial area require inverse interpretation of magnetic maps, as a result of this a survey carried out at equatorial area require either reduction to pole or reduction to equatorial that simplify the interpretation of the magnetic anomaly.

Transforming magnetic anomalies observed at low magnetic latitudes to those that obtained if surveys have been taken at the magnetic poles decidedly simplify the interpretation of magnetic anomalies. This possibility exists by using a mathematical method known as reduction to pole (Abera Alemu, 2020).

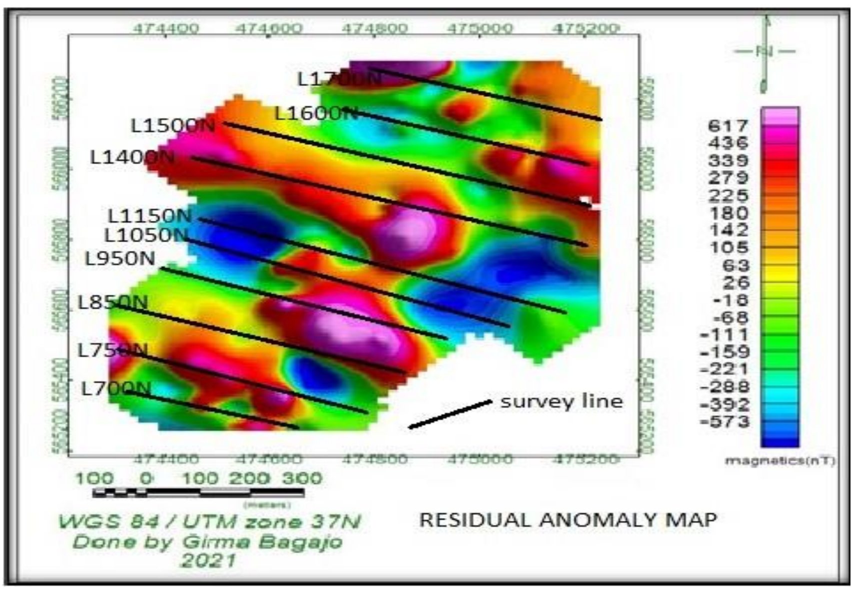

Figure 5.2. Residual magnetic field anomaly map

D) REDUCED TO EQUATORIAL RESIDUAL MAGNETIC ANOMALY

Magnetic field intensity at the equatorial is smaller and induces magnetic field oriented in horizontal direction. If the data are collected at equatorial, anomalies over magnetically susceptible materials depict negative values instead of positive values. This results in complication of interpretation. Figure (5.3) is reduced to equatorial residual magnetic field anomaly map which shows a little modification from residual anomaly map. In contrast to reduction to pole, reduction to equatorial filter is quite stable irrespective to latitude and the advantage of this filter is that it centers anomalies over their respective source, even if anomaly stretched in east to west direction (geological survey of Norway, 2000).

Reduce to equatorial magnetic anomaly map of Okote prospect area reveals, high magnetic anomaly at Northeast, Northwest, southeast and central of zones the area, while low magnetic anomaly is situated at Northwest, East and west of the study area. Three profile lines are place on the map to show the position and direction from which the models discussed in the next portion were taken.

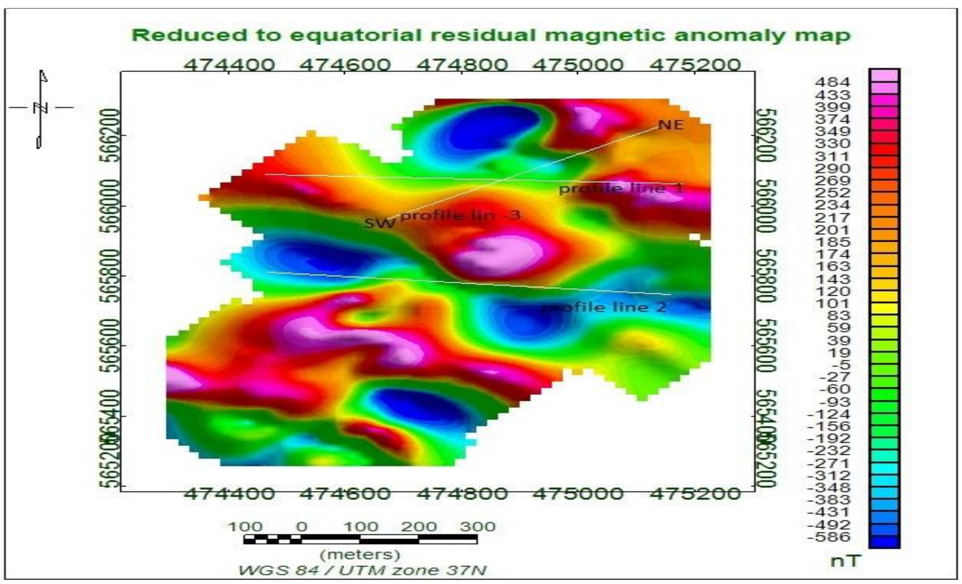

Figure 5.3. Reduce to equatorial residual magnetic anomaly map

E) ANALYTICAL SIGNAL MAGNETIC ANOMALY MAP

Analytical signal is total gradient applied to magnetic anomaly of interest. Since shallow depth is desired zone for mineral exploration analytical signal map (figure 5.4) is derived from residual anomaly grid. It comprises of both vertical and horizontal derivatives and depicts magnetized body in the contacts regardless of considering low latitude effects on the magnetic anomaly.

Positive analytical signal values imply presence of the contacts hosting magnetic materials. The following analytical signal magnetic anomaly map is interpreted into two main geological contacts of high magnetic anomaly. These two main contacts are oriented to NW-SE and NE-SW directions. The wider anomalies contact located at the northwest of study area indicate a presence of deep-seated geological contact.

Generally, analytical signal map (figure 5.4) which derived from residual magnetic anomaly grid reveals existence of high magnetic susceptibility contrast across the contacts and the two above mentioned orientation of the contacts are indicated on the following analytical signal map.

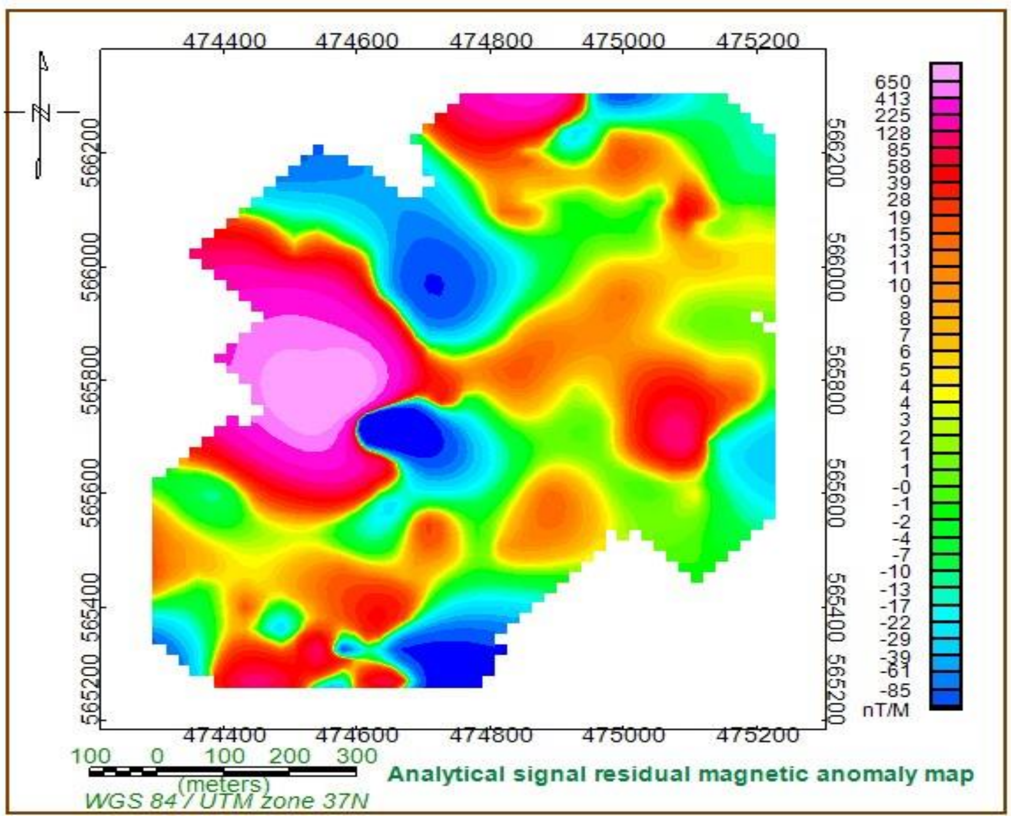

Figure 5.4. Analytical signal magnetic anomaly map

F) TILT DERIVATIVE OF RESIDUAL MAGNETIC ANOMALY MAP

Tilt derivative enhancement method is one way of qualitative interpretation of magnetic anomaly, which emphasis on location of fractures and contacts. It depicts faults and anomalies geological contacts in detail when compared with the rest anomaly enhancement methods.

Tilt derivative magnetic map (figure 5.5) is derived from analytical signal of residual magnetic anomaly grid and it indicates clear trends of geological structures. Faults which do not indicated on a signal analytical map are displayed on it. Especially, structures mapped around west of study area, which does not identified by analytical signal method are clearly mapped. NE to SW and NW to SE trending structures are the main geological structures of the area. Structures of NW to SE trending are dominantly distributed within the area as it seen from the following map (figure 5.5).

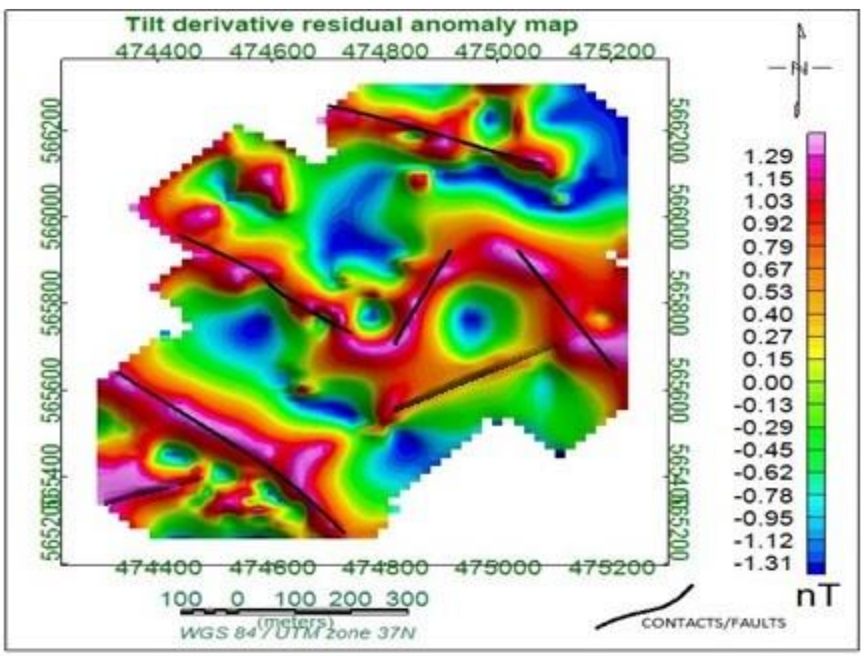

Figure 5.5 Tilt derivative of residual anomaly map

G) EULER DECONVOLUTION OF RESIDUAL MAGNETIC ANOMALY MAP

Figure (5.6) is euler deconvolution map of okote prospect area's residual magnetic anomaly which is used to range geological features and structures distribution with respect to the depth and lateral extension of the survey area. As indicated on the map, distributions of geological features and structures are dominated at NW and SE zones of survey area. Shallow depth geological structures reveal NE-SW and NW-SE orientations, and structures at the depth ranges from 50m to 80m are also reveal similar orientations. The clustering of the circles at both above mentioned depth ranges show linear trending of structures; however it does not show significant linear clustering at the depth ranges beneath 80m.

Generally there is no significantly mapped geological structure at the depth ranges less than 15m. Distributions of structures are mostly concentrated at 15m to 80m depth and its concentration is decreased gradually beneath 80m depth.

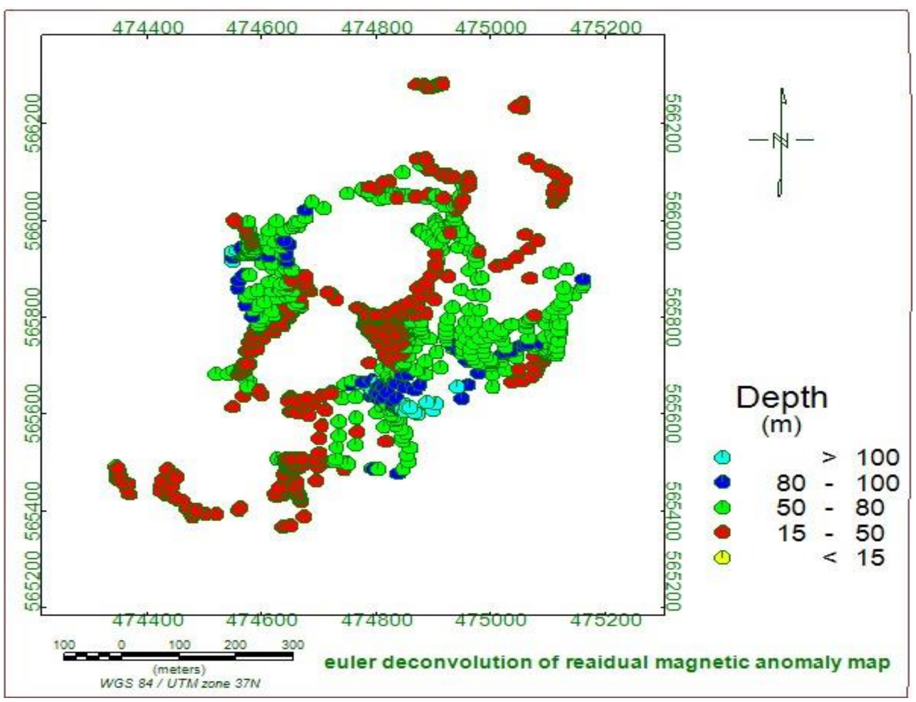

Figure 5.6. Euler deconvolution of residual magnetic anomaly map for SI=1

5.2. TWO-DIMENSION FORWARD MAGNETIC ANOMALY MODELING

The following 2D magnetic anomaly models are derived from profile lines portrayed on the filtered residual magnetic anomaly map (RTE). Two of the models are performed from profile lines which are oriented to east-west direction, whereas the rest one is from profile line oriented NE to SW direction. The aim of the models is to depict geology and geological features with its respective magnetic anomaly along the selected profile lines and the depth.

I. MODEL-1

This model is derived from profile line -1 which is indicated on the reduced to equatorial residual anomaly map. Three lithological variations are displayed on the model and different litho-contacts with respect to the depths also indicated on the model. Metagabbro, chlorite actinolite schist and carbonate chlorite schist are three main rocks which are displayed on the model. High magnetic anomaly is exist at east and west of the model and one penetrative fault is located in between high and low magnetic anomaly revealed at east of the model. The lithological variation of the area are known from integrated data of both drill hole log, and inverted section of resistivity and chargeability.

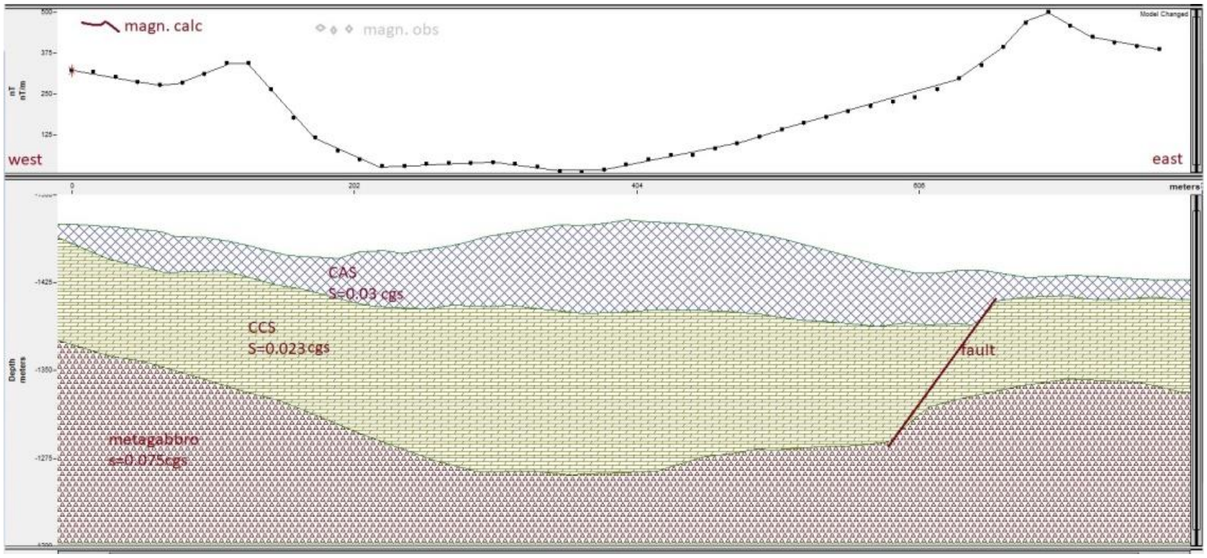

Figure 5.7. 2-D model-1 from profile line one

II. MODEL-2

Model-2 is derived from profile line-2 that depicted on the reduced to equatorial residual anomaly map as indicated on the figure 19. This profile line oriented to east-west direction within low magnetic anomaly zones. The aim of a model is to portray this low anomaly zones and geological features along selected profile line with respect to the depth. Three different lithological variations are displayed on the model and different litho-contacts with respect to the depths are also indicated. Similar to the above mentioned model, this model depict high residual magnetic anomaly where low susceptibility earth materials are exist and vice versa.

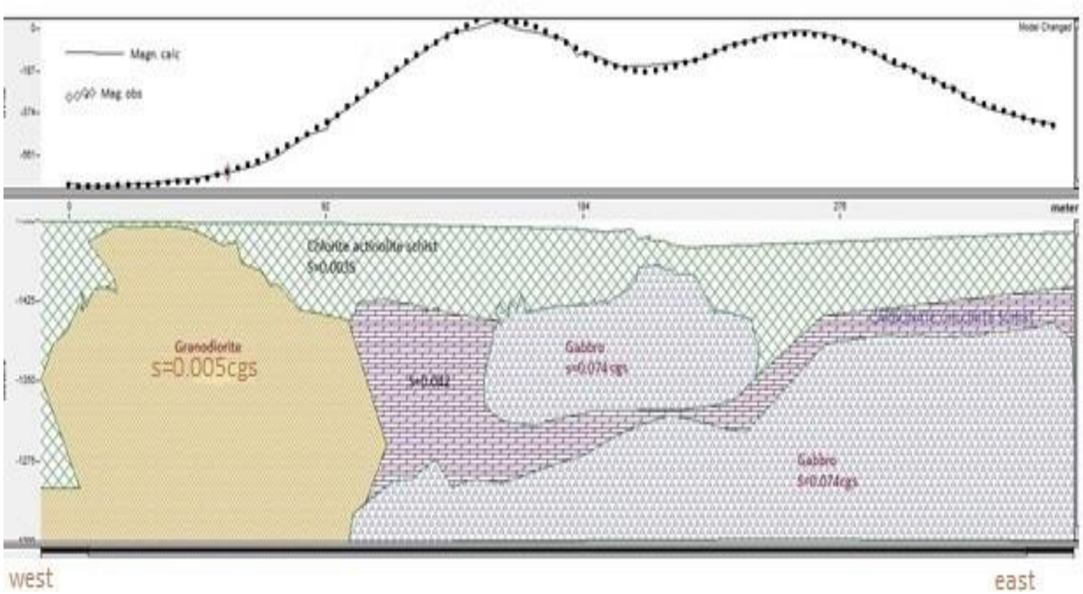

Figure 5.8 model-2 from profile line-2

III. MODEL-3

Model-3 is derived from profile line-3 that portrayed on the reduced to equatorial residual magnetic anomaly map. This Profile line indicates NE to SW orientation as it is depicted on the figure (5.3). Three different lithological variations which tectonically unstable are displayed, and different litho-contacts and penetrative normal dip slip fault are indicated on the model. The model indicates conformity of residual magnetic anomaly profile and magnetic susceptibility of the earth materials directly below profile lines. Low susceptibility earth materials are located below low magnetic field anomaly and vice versa. This consistence of the magnetic anomalies profiles and magnetic susceptibility of the subsurface materials directly below respective anomalies is due to that the model is derived from filtered residual magnetic anomaly map (RTE).

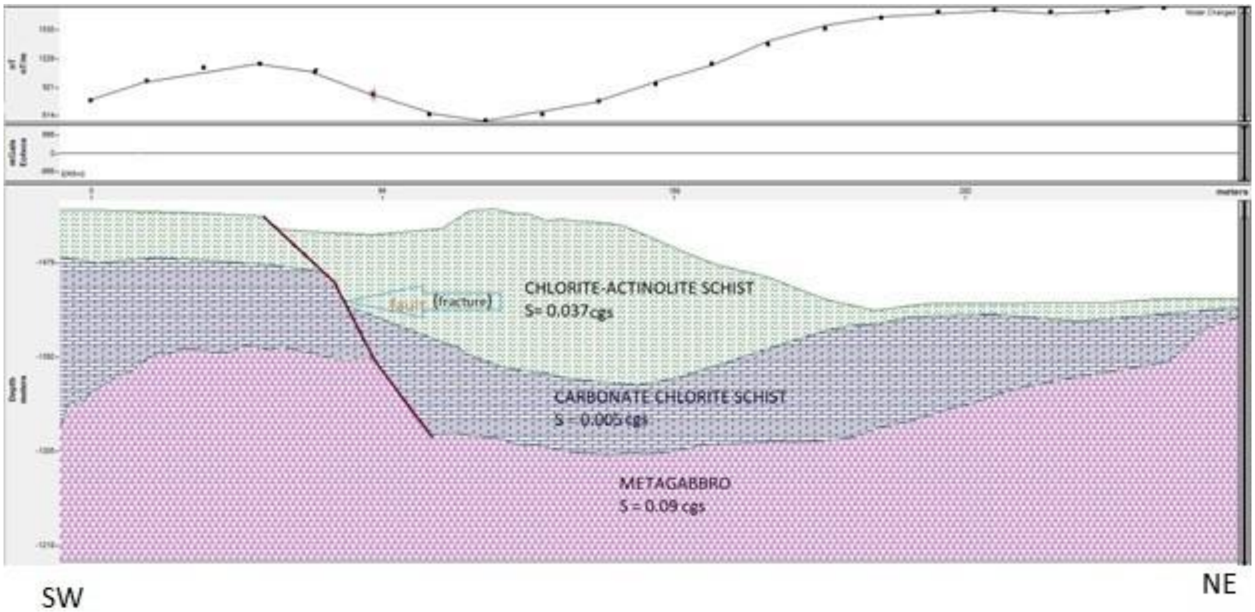

Figure 5.9. 2D model-3 for the profile line 3 on RTE residual anomaly map

5.3. INTERPRETATION OF RESISTIVITY AND CHARGEABILITY PLAN MAPS

5.3.1. DIPOLE – DIPOLE ARRAY

I. PLAN MAP of n-1 LEVEL

Apparent resistivity and chargeability plan maps of n_1 - spacing are given in Figure (5.10). The n-1 resistivity map shows low resistivity zones at the southwest, south and northeast part that are denoted by RD, RF and RE respectively, whereas it shows High resistivity zones mapped at the west, north and east zones of the northern part of the plan map marked by RA, RC and RB. Resistivity map zones denoted by RA, RE, RD and RF are opened anomalies of survey area.

Chargeability map of n_1-level (figure 5.10) reveals three high chargeability zones at the northeast to southeast, northwest and southwest part of plan map which is leveled by A, B and C letters and low chargeability zones are displayed at the area marked by D, E, F and G letters.

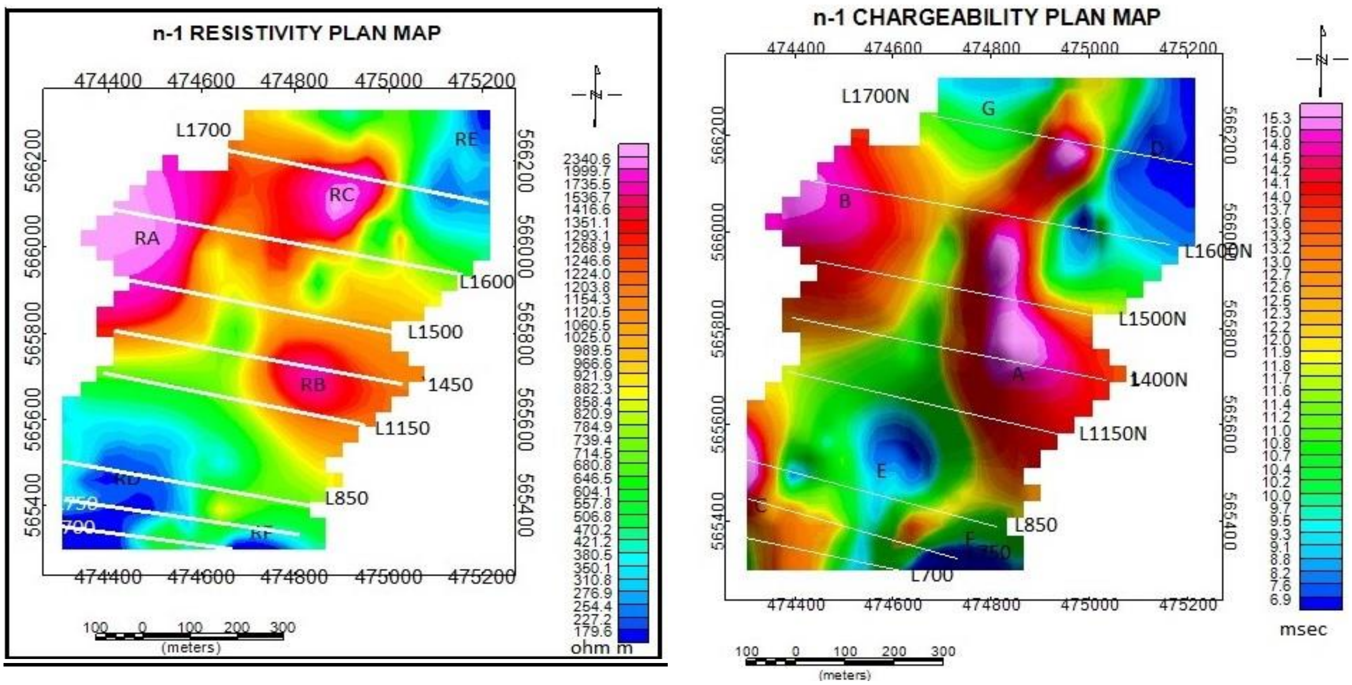

Figure 5.10 N-1 level chargeability and resistivity plan map

RA, RB and RC denoted zones on resistivity plan map and A & B denoted zones on chargeability plan maps are correlated as high resistivity and high chargeability area. RE and RF on resistivity plan map, and D, E & F marks on chargeability plan map show low resistivity and low chargeability anomalies correlation, however RD and western top of RE on resistivity plan map and C and G levels on chargeability plan map indicate low resistivity and high chargeability correlation.

II. PLAN MAP OF n_2-LEVEL

Apparent resistivity and chargeability given as a figure (5.11) indicate four different anomalies contrasts zones (high- high, low - low, high- low and low-high) of resistivity and chargeability anomalies similar to above mentioned plan map. High resistivity and high chargeability zones are wider when compared with rest zones of resistivity and chargeability contrast. Resistivity plan map of n2 is marked as “RA, RB, RC, RD, RE and RF”, and chargeability plan map is marked as “A, B, C and D” for the sake of simplifying interpretation of the anomaly zones.

Wider area in the northwest of the map indicates the presence of high resistivity and high chargeability, whereas the little zones on the southwest and northeast reveal the presence of low anomalies for both resistivity and chargeability. This plan map rarely indicates existence of an offset (inverse proportionality) of resistivity and chargeability anomalies for the same area.

A zone marked as “RA” on a resistivity plan map which is limited to NW of a plan map and confined within 1150N and 1600N survey lines shows high resistivity and high chargeability, whereas the zones in vicinity of “C and D” on chargeability plan map depict low resistivity and intermediate to high chargeability. The regions “B” on both plan maps display intermediate to high resistivity and low chargeability. Northeast portion of both map have low anomalies, while a southwest zone shows dispersed anomalies.

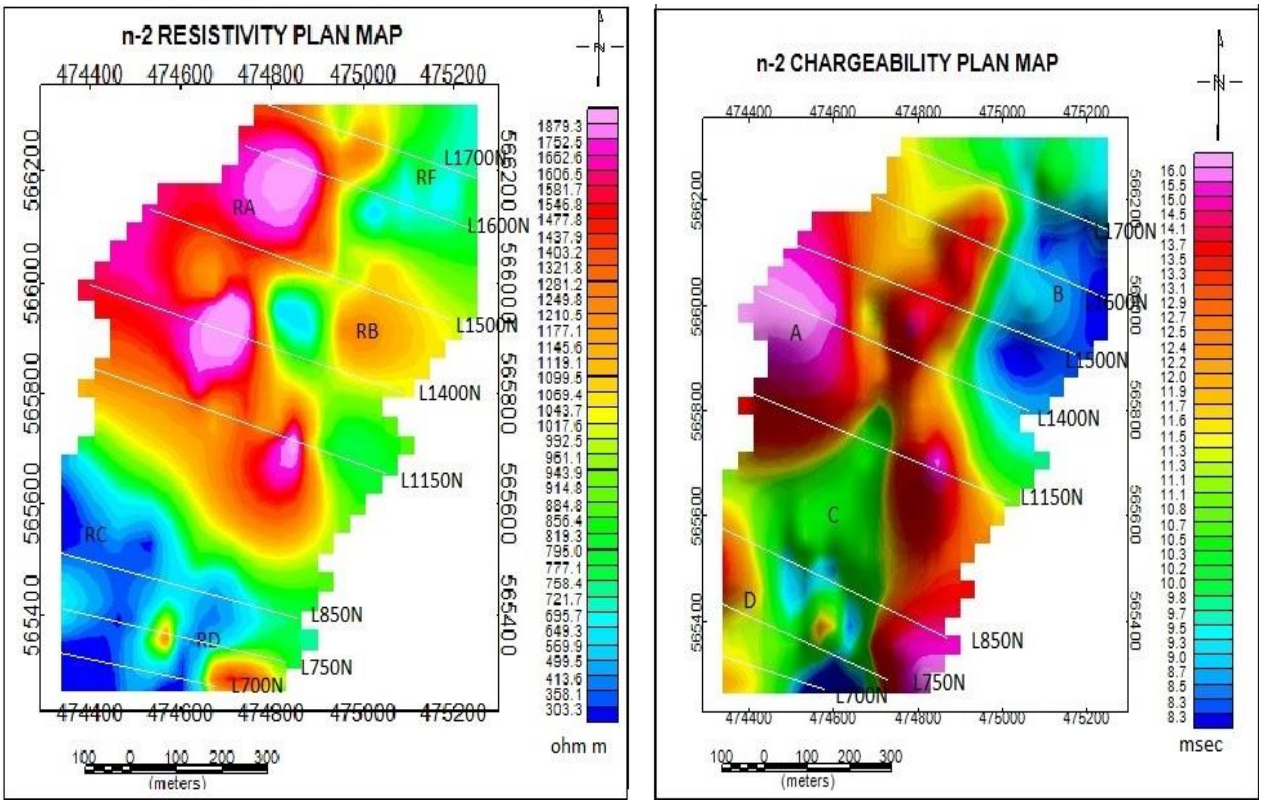

Figure 5.11. N-2 level chargeability and resistivity plan map

III. PLAN MAP OF n_4 - LEVEL

Apparent resistivity and chargeability plan maps for n_4 - spacing are given in Figures (5.12). The N-4 resistivity map shows low resistivity at the North, south and central part of study area that are denote by RA, RB and RC respectively, whereas it shows three High resistivity zones mapped at the west, South and east zones of the plan map marked by RE, RF and RD. High resistivity anomalies indicated at the east and west of the area are opened anomalies at n-4 level.

Chargeability map of n_4-level (Figure 5.12) reveals three high chargeability zones at the northwest, northeast and southeast parts of plan map which are denote by A, B and C letters. Low chargeability plan map is displayed at north, east and southwest around the area marked by D, E, and F letters.

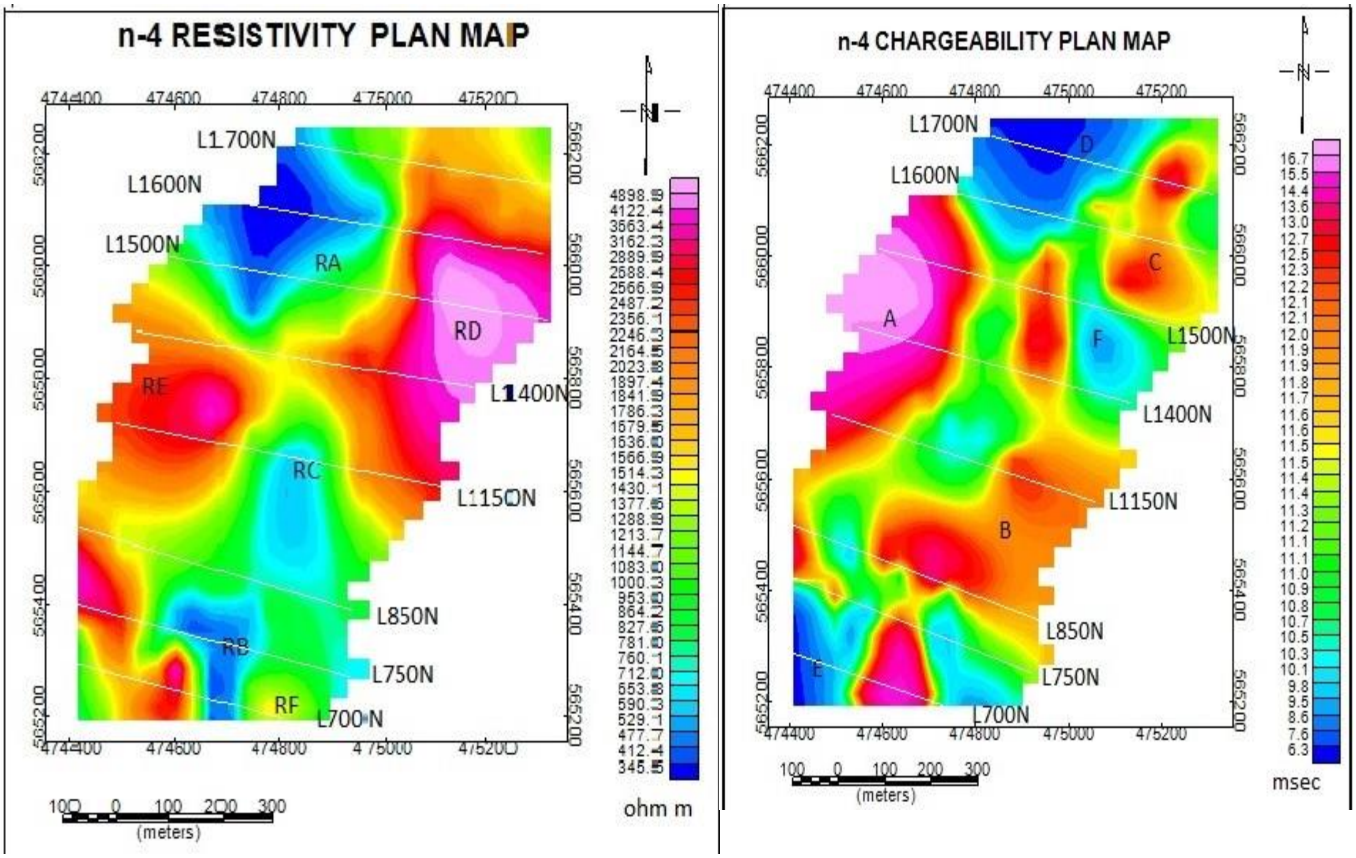

Figure 5.12. n-4 level chargeability and resistivity plan map

IV. PLAN MAP OF n_6 - LEVEL

Apparent resistivity and chargeability plan maps for n_6 - spacing are given in Figures (5.13). The n-6 resistivity map shows low resistivity zones at the west, east and northeast that are marked by RD, RE, RF and RG, whereas it shows three High resistivity zones mapped at the west, north and east zones of the northern part of the plan map which are marked by RA, RB and RC letters. These zones cover half of plan map area. Resistivity maps indicated by RA, RE, RD and RF are opened anomalies of n-6 level.

Chargeability map of n_6-level (Figure 5.13) reveals high chargeability zones, which cover wide area at southern portion of plan map, and northeastern area, that are denote by A, B, C, D, E and F letters. Low chargeability map is displayed at the area marked by G, H, K and L letters.

High resistivity zones at southern and north eastern part of plan map depict corresponding high chargeability anomalies. High chargeability zones marked by B, D, F and small area between A and C on chargeability plan map indicate low resistivity of the same area. However a

The zones marked by G, I, K and H are low anomalies area on both plan maps. Very limited area shows high resistivity and low chargeability for the same area.

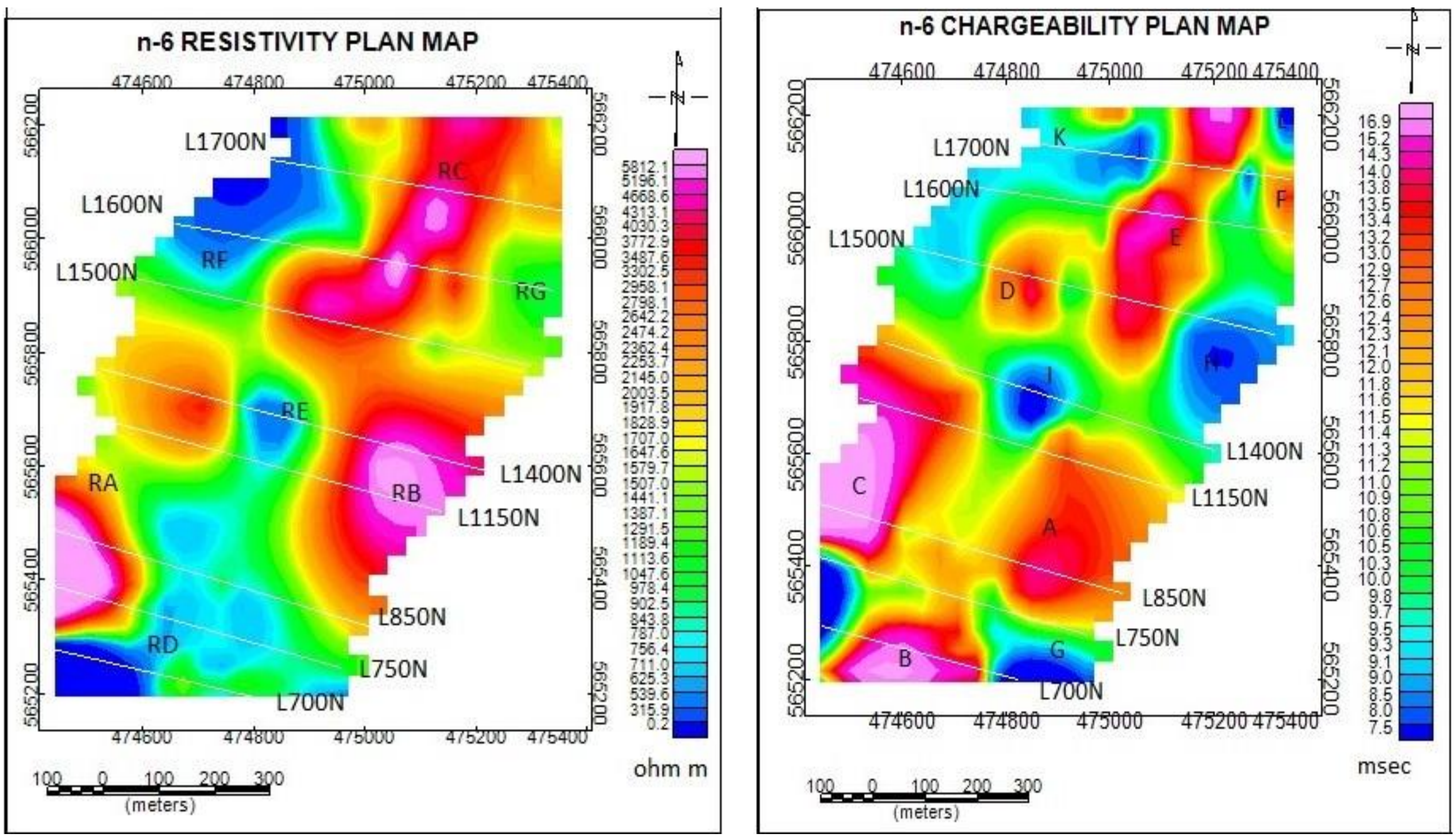

Figure 5.13   n-6 level chargeability and resistivity plan map

5.3.2. GRADIENT ARRAY

Figure 5.14 and 5.15 show resistivity and chargeability maps of the Gradient array data collected from two survey lines (950N and 1050N). These two survey lines are located at southern part of prospect area.

The maps reveal high chargeability at A, B, and C marks on chargeability map (figure 5.15) and high resistivity map at A, B and C marks on resistivity map (figure 5.14), however it show relatively low resistivity at D, E, F, G and H and low chargeability at D, E, F and G marked zones.

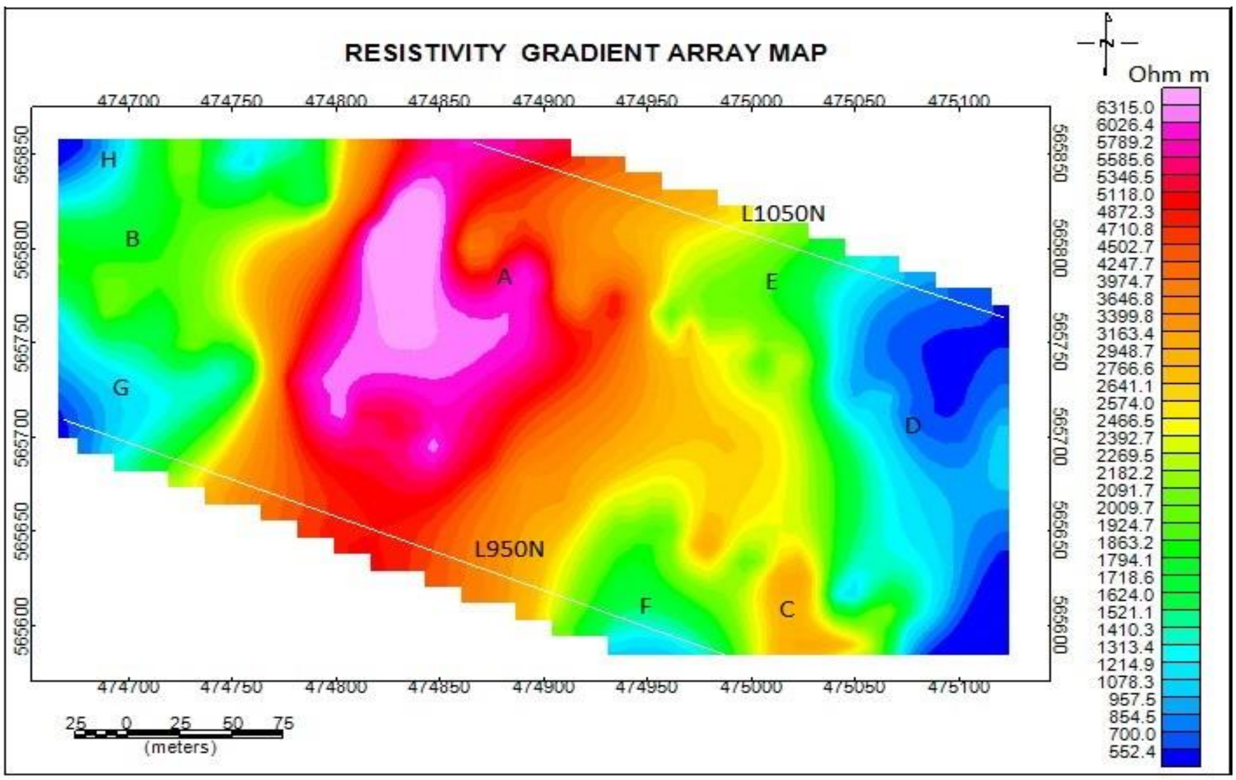

Figure 5.14. Gradient array resistivity map between line 950N and line1050N

High chargeability zones are dominated in west of a map which shows an opened high chargeability anomaly to the southwest direction. Most of these zones are elongated in NE-SW direction. Line 950N is crosses high chargeability zones on its west side whereas line 1050N does not cross it. As it is evidenced from geological map of Okote that is indicated in chapter two, the western part of line 950N is dominated by quartz veins, quartz carbonate veins, silicification zones and metagranodiorite rocks which are concisely correlated with high chargeability zones.

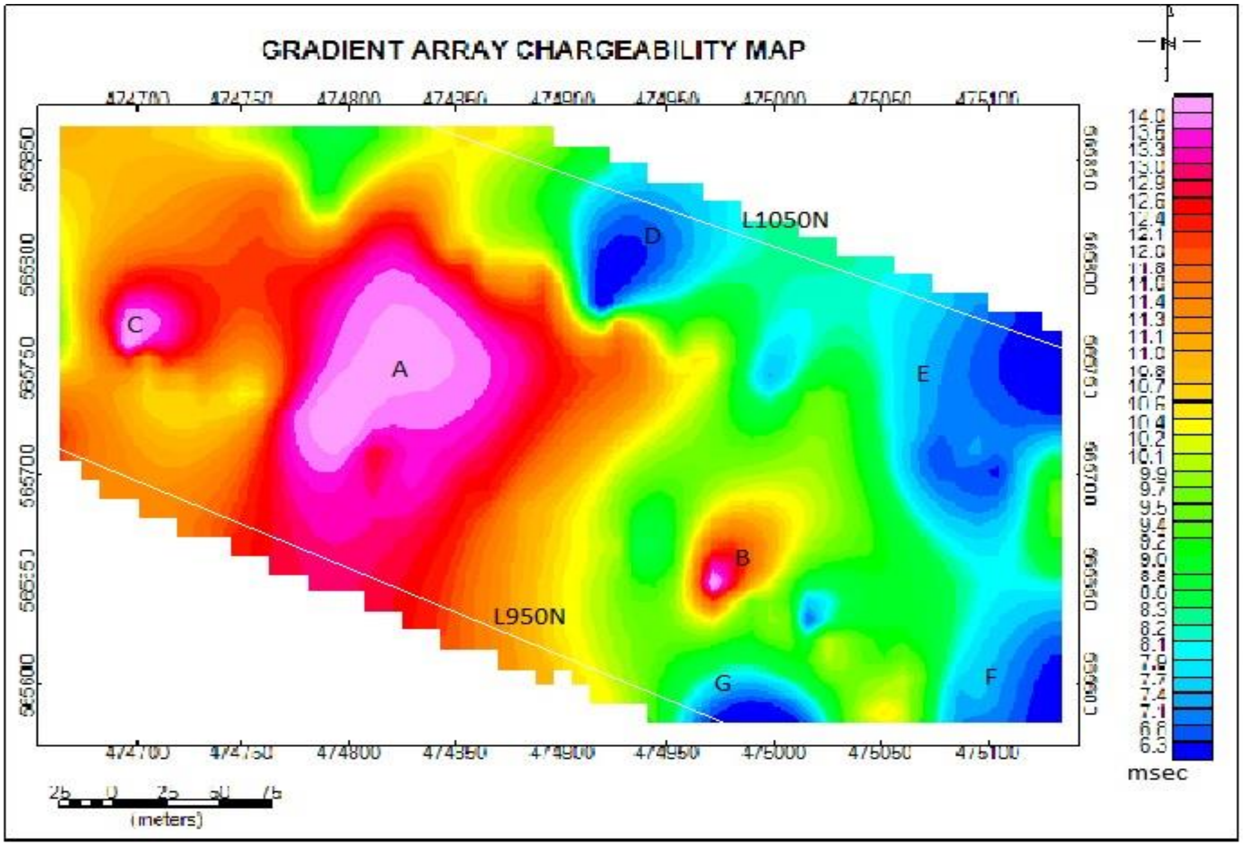

Figure 5.15. Gradient array chargeability map between line 950N and line1050N

5.4. INTERPRETATION OF RESISTIVITY AND CHARGEABILITY INVERTED SECTIONS

Resistivity and chargeability data is inverted using RES2DINV computer program which automatically displays the two-dimensional models for the subsurface data obtained by electrical imaging surveys.

5.4.1. RESISTIVITY AND CHARGEABILITY INVERSE MODEL FOR 700N SURVEY LINE

Inverse model of resistivity (figure 5.16) reveals that low resistivity earth materials are situated up to 45m depth in the limits of x- location bounded between -900m and -650m. The massive high resistivity materials are located beneath low resistivity on the left side of the model below 45m depth. It is extended down ward without finitely terminated within 149m depth. This high resistivity homogeneous body is interpreted as an intrusion of metagranodiorite which is a cause for mineralization as evidenced from drill hole log (DH700N/1). As it is possible to be observed from resistivity model there are many fractures and dykes in the area which are emanate from an intrusive. The most possible extensive and penetrative faults are located on left and right termination of high resistivity body. These faults show NW-SE trending of approximately 45 degree dip angle.

Inverse chargeability model (figure 5.16) indicates the presence of high chargeability zones on right side of litho-contact. This zone is situated beneath the x- locations which range from -570m to -270m and it shows continuity of the anomaly with respect to the horizontal and the depths. A zone of high resistivity which is interpreted as an intrusive indicates a low chargeability.

As evidenced from geologic drill hole log (DH700/1) located at 474592E and 565266N low resistivity zones extended from 15m to 50m depth are correlated to chlorite actinolite schist invaded by dykes while, a massive high resistivity intrusive body is correlated to metagabbro/amphibolite. The schist reveals an intermediate to high chargeability, whereas metagabbro shows low chargeability.

Generally, chargeability anomalies increase outward from low conductivity intrusive body which squeezes the country rocks in all direction. An intrusion does not mineralized for itself; rather it is act as a source for the hydro thermal fluid and mineralization. Therefore fracture filling mineralization is a style of mineralization identified from this inverse model sections.

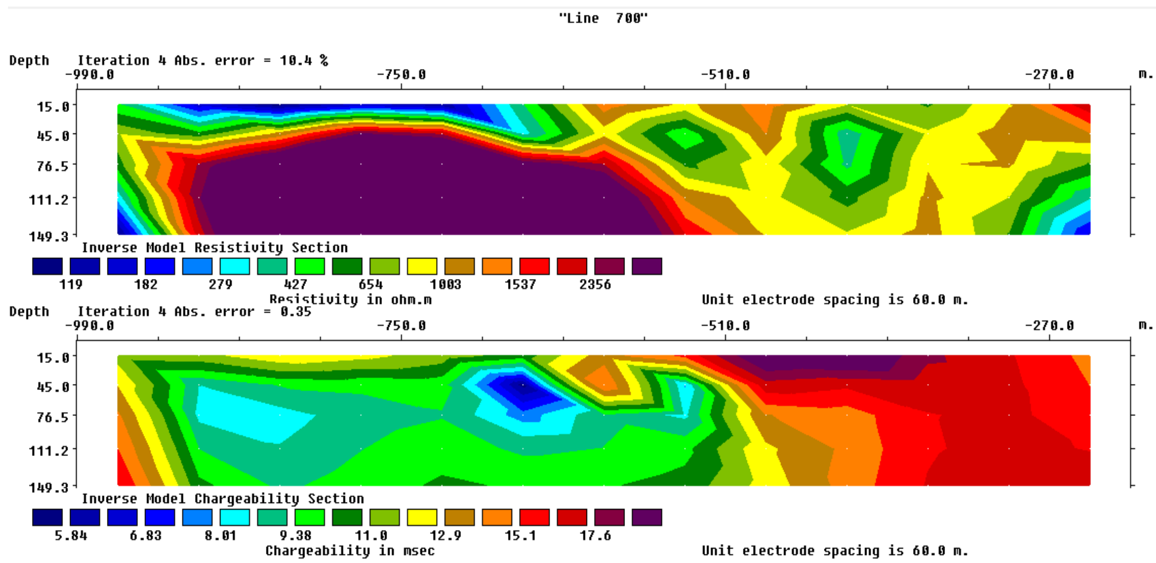

Figure 5.16. Inverse model of resistivity and chargeability for line 700N

5.4.2. RESISTIVITY AND CHARGEABILITY INVERSE MODEL FOR 750N SURVEY LINE

Line 750N resistivity and chargeability inverse model section resembles with that of the line 700N. Resistivity inverse model of line 750N (figure 5.17) shows low resistivity on the top most portion of inverse model which is thicker than that of line 700N inverse model.

Each layers situated at the left part of model section shows an offset of the layers. This offset of the layers is interpreted as a fault that shows NW-SE trending and it reveals the same orientation with the high and low resistivity contacts. The depth to the homogeneous competent lithology is increased from 45m to 75m when compared with 700N previously inverted map. The rest area of this inverted map shows low resistivity which increases in resistivity towards to competent intrusive rock.

A zone of massive and competent intrusion reveals low chargeability (7msec –12msec) including low resistivity zones overlaid competent intrusive body, regardless of locally limited high chargeability area on top left corner of the inverse model. However the right side of inverted section increases in chargeability starting from contacts that located at -

510m on x-location. There are the series of different chargeability columns which are increase in size and chargeability on the east of the contact.

Generally, this inverse model shows low chargeability anomaly when compared with chargeability of line 700N inverse model and this indicates a little mineralization of sulfide minerals.

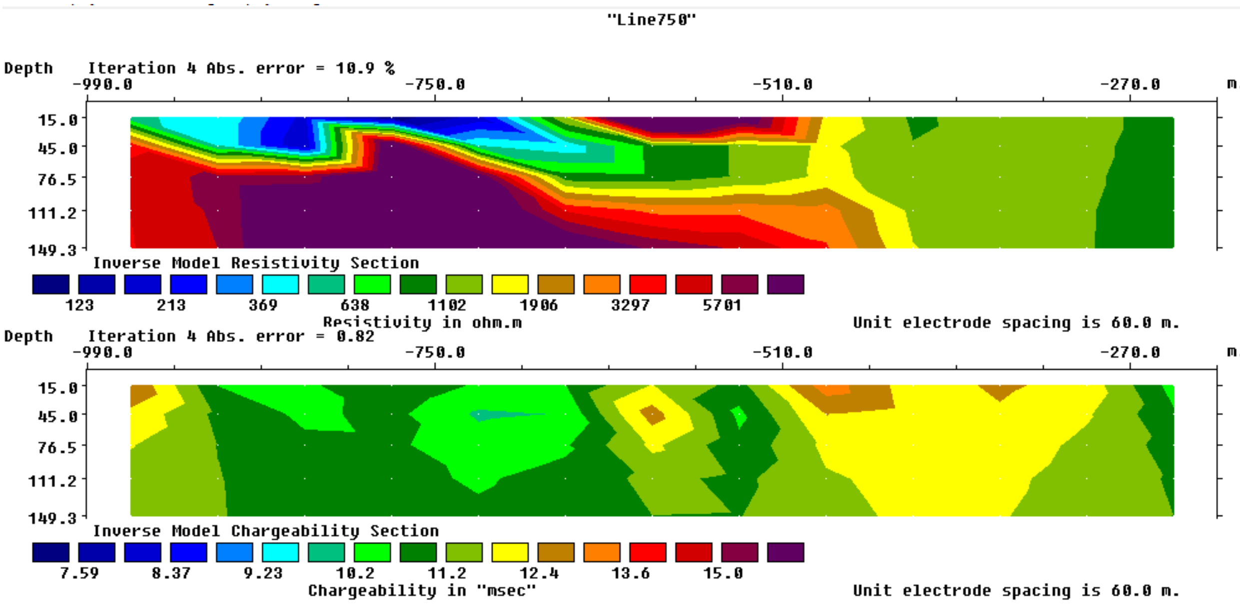

Figure 5.17. inverse model of resistivity and chargeability for line 750N

5.4.3. RESISTIVITY AND CHARGEABILITY INVERSE MODEL FOR 850N SURVEY LINE

Figure (5.18) is resistivity and chargeability inverse model of pseudo sections along 850N survey line. This resistivity inverse model resembles the resistivity inverse model of the line 700N and 750N except for particular locations that show the little deviation.

Low resistivity materials are located on entire top most portion and right side of inverse model. This low resistivity situated on the top portion of intrusive body does not show equal thickness as a result of the dip slip fault that disturbs horizontality of the layers.

The low resistivity materials overlay homogenous high resistivity body that opened (continued) down the depth and to the left of the map. It forms a vertical contact with the country rock at about -510m on the horizontal distances. Another younger fault is entirely cross cut this competent rock and overplays layer. It is dip at angle with NW to SE orientation which shows upward movement of hanging wall relative to fault plane. This dip slip fault is reverse fault as it is understood from relative movement of foot wall and hanging wall with respect to the fault plane.

Chargeability inverse model show varies vertical and horizontal layering. Intrusive body reveals low chargeability that increases with the depth on the left of vertical contact. Chargeability is high at the right side of the contact and it is increases laterally away from the contact. This High chargeability section indicates strati-form mineralization which shows disseminate style of mineralization. There is no implication of structural controlled mineralization in this inverse model.

As evidenced from drill hole (DH850N/1) that located at 474676E and 565387N on the survey line, the low resistivity layer which overlay a homogenous intrusive body is correlated to the alternative intercalation of chlorite actinolite schist and metagranodiorite which is extended from 15m to 60m depth. The top most layers up to 15m depth do not incorporated within this inverted section. Even though no drilled hole exists, the right side low resistivity zones are correlated to schist. The massive high resistivity intrusive body is concisely correlated to metagabbro.

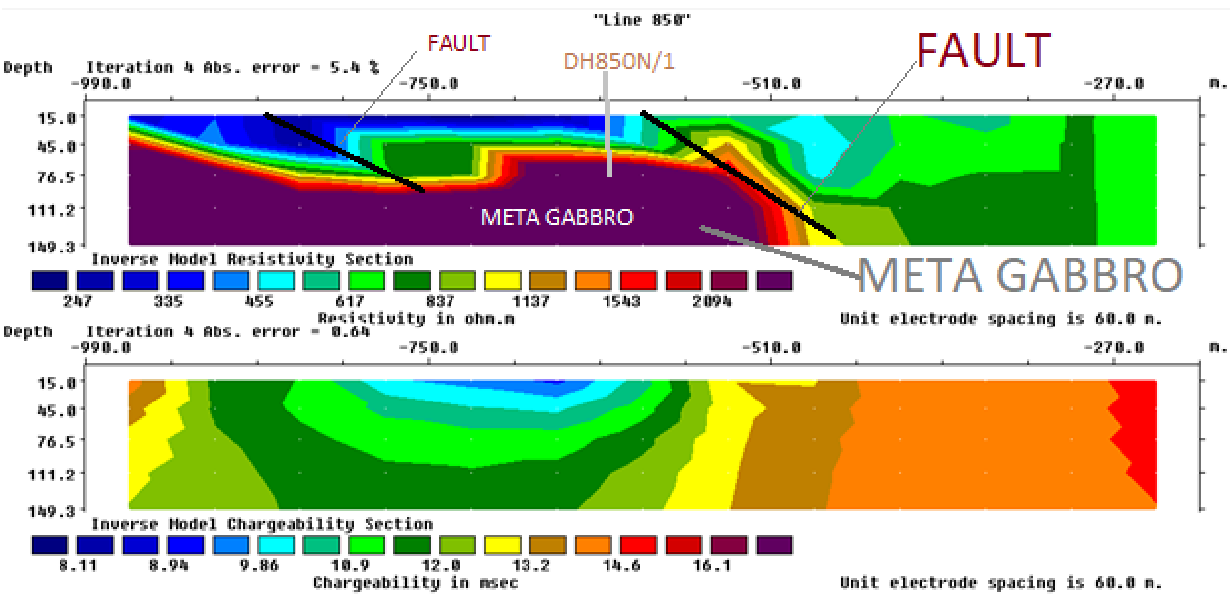

Figure 5.19. Inverse model of resistivity and chargeability for line 850N

5.4.4. RESISTIVITY AND CHARGEABILITY INVERSE MODEL FOR 1150N SURVEY LINE

Figure 5.20 show low to high resistivity anomaly. High resistivity zones are concentrated at east and west of an inverse model. The west portion show rounded shape which slightly elongated in NW to SE direction and dipping with an angle. However the right portion of high resistivity zone is huge and infinitely extended laterally and vertically. This zone is increases in size towards to 1400N survey line and interpreted as an intrusive body. Locally limited intermediate resistivity zones which have the same orientation with left side enclosed and elongated anomalies body are located at the middle portion of inverted section.

The map host promising chargeability anomalies and these high chargeability anomalies are related to structurally controlled mineralization. A dyke that situated on the left part of inverse model is mineralized and host high resistivity and high chargeability correspondence. The right side implication of mineralization which situated in vicinity of -270m on x-location is related to the contact between intrusion and country rocks. An intrusive body shows high resistivity and low chargeability. This indicates that lack of sulfide and associated minerals. The dykes show direct proportionality of resistivity and chargeability on both sites. This may be correlated to silicification and granodiorite rock which host chargeable minerals.

As evidenced from geologic drill hole log (DH1125N/2) that located at 474741E and 565670N around the survey line in vicinity of -710m on horizontal distance, relatively low resistivity zones (<2000Ωm) are correlated to chlorite actinolite schist and slightly altered zones of the same lithology. These zones show almost all high chargeability which reveals sulfide mineralization. The right side and central intrusive body which show intermediate to high resistivities (2500Ωm -5500Ωm are correlated to metagabbro, however the high resistivity intrusive body on the left portion of inverted section is mineralized zone. This intrusive body does not correlated to existing geological drill hole log data, because it shows unique properties to be correlated to it, however based understanding of previous properties of lithology, this zone is interpreted to be metagranodiorite as it shows high resistivity and high chargeability anomaly.

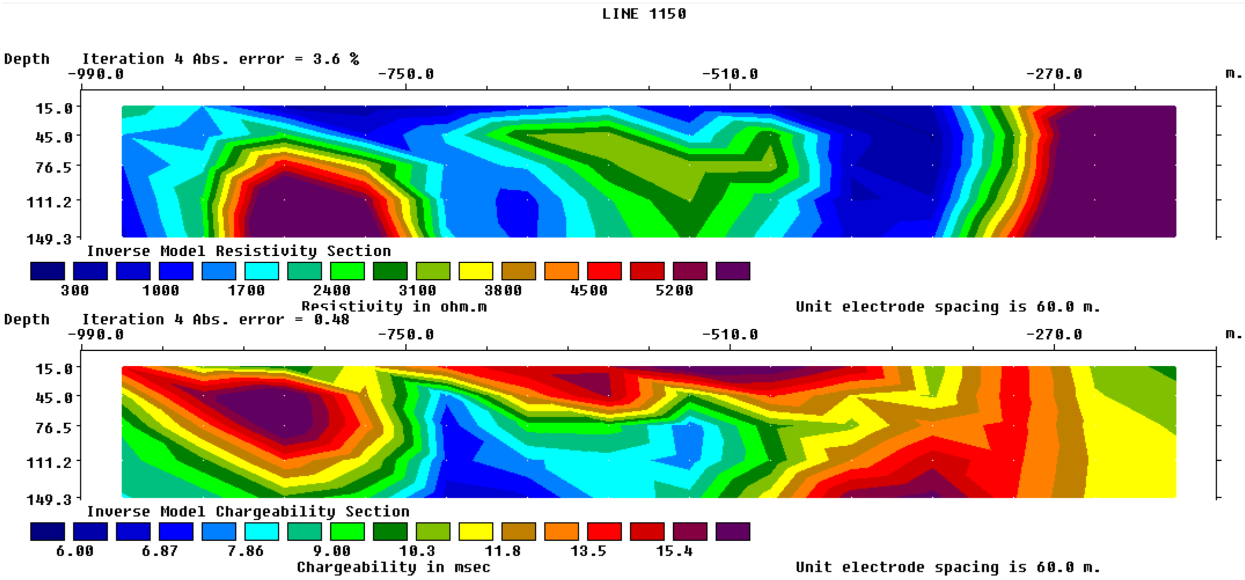

Figure 5.20. Inverse model of resistivity and chargeability for line 750N

5.4.5. RESISTIVITY AND CHARGEABILITY INVERSE MODEL FOR 1400N SURVEY LINE

Resistivity and chargeability inverse model of this survey line resembles the previous inverse model of 1150N survey line. High to low resistivity materials are identified on the left part of inverse model and high resistivity homogeneous earth materials are existing on the right portion of inverse model. Intermediate to high resistivity lineament dipping due to southeast is interpreted as a dyke and it is cross cut low resistivity material in to northeast and southwest sections. This dyke is prospected as a promising site for structural controlled mineralization and reveals intermediate to high resistivity value ranging from 3000Ωm to 5000Ωm. It shows direct proportionality of resistivity and chargeability.

Low resistivity material which enclosed between two fault zones reveals high chargeability on its top most portions and is prospected as promising site for significant mineralization. It is situated at about -500m to -320m on x- location and shows 45m thickness. One vertical drill hole up to 100m depth is proposed at -580m on horizontal distance to check for mineralization of right bottom extension of a dipping dyke which have intermediate chargeability at a depth.

As it is confirmed from geological drill hole log (DH1400/1) data collected from drill hole located at 474749E and 566016N around -580m on x-location, the low resistivity zones (<800Ωm) are correlated to carbonate chlorite schist, chlorite amphibolite schist and quartz veins. Metagranodiorite is located at top most of all layers and it shows a small thickness layer confined between -500m and -340m on horizontal distances that reveals high chargeability. NW to SE oriented dyke also correlated to meta-granodiorite.

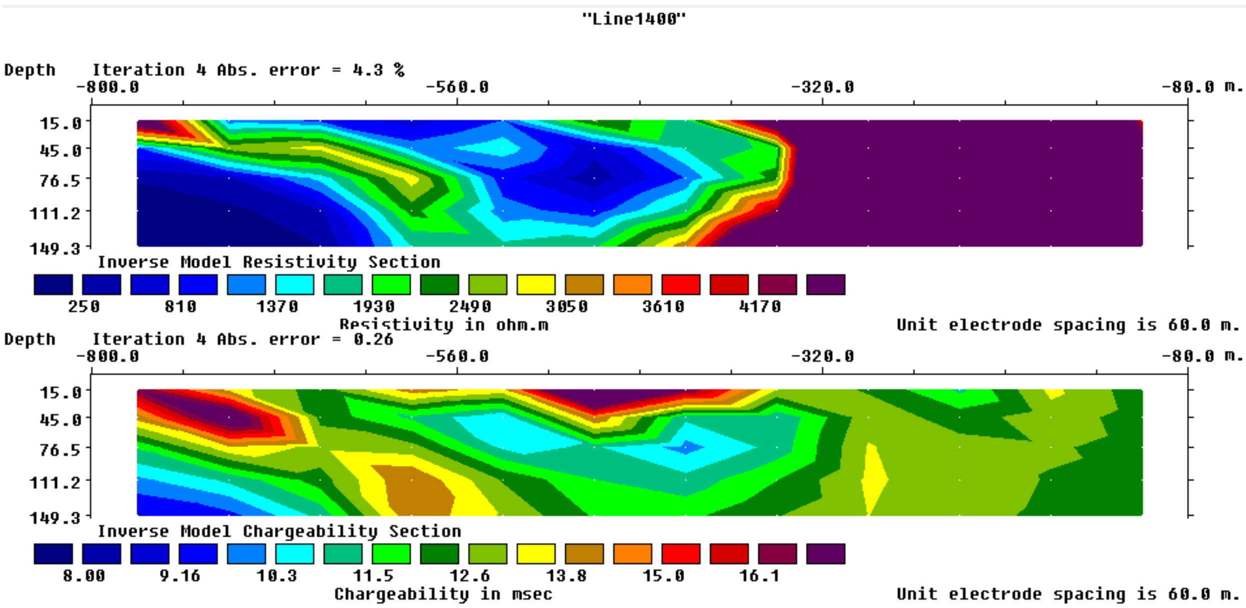

Figure 5.21. Inverse model of resistivity and chargeability for line 1400N

5.4.6. RESISTIVITY AND CHARGEABILITY INVERSE MODEL FOR 1500N SURVEY LINE

Line 1500N inversed resistivity pseudo section shows 3 major resistivity variations. These variations are low resistivity zone, high resistivity zone and intermediate resistivity zone when mentioned from left to right on inverted resistivity map. These three different lithologies are situated at the various horizontal distances and are separated by vertically penetrative contacts at -620m and -170m x-location. The left most contact is gradual contact whereas the right side one is sharp contact. Each of these three lithologies does not show homogeneity. Low resistivity zones host locally high resistivity materials enclosed on top most of the zone and reach up to 50m depth within limited x-location from -700m to -560m. This material is buried by thin overburden that has about 20m to 45m thickness.

Chargeability of the same map shows low and high chargeability zones. Low chargeability zone is found between -560m and -320m on horizontal distances whereas high chargeability zones are located on both side of this low chargeability anomaly zones which reveal horizontal chargeability layer indicating increase of chargeability with the depth. Even though it shows increasing of chargeability with the depth, the zone is going to pinch out within a few depths below 149m. This zone is bounded between two normal faults that trend at angle to the depth.

The left side anomaly bodies show vertical chargeability variations that decrease with a depth whereas the right side high chargeability shows horizontal chargeability variation that increase towards to the last electrode on right side. This high chargeability is opened down ward and right side of a survey area.

There is no nearby drill hole log data to be correlated to inverse model of 1500N survey line. However the map shows a little similarity to next inverted section of 1600N survey line.

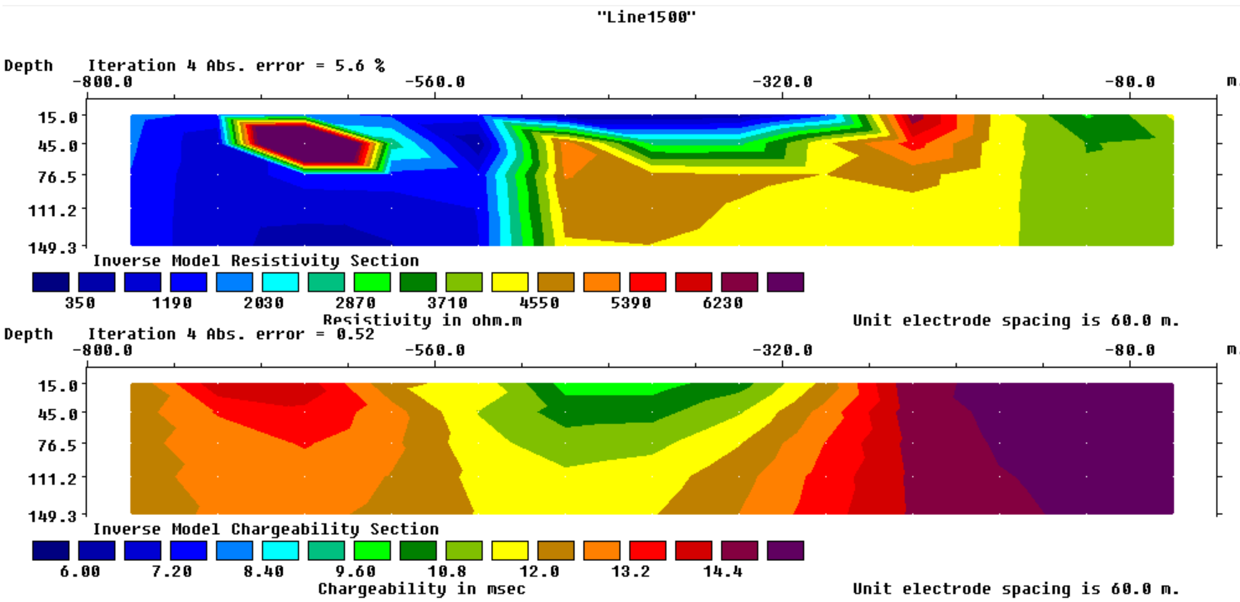

Figure 5.22. Inverse model of resistivity and chargeability for line 1500N

5.4.7. RESISTIVITY AND CHARGEABILITY INVERSE MODEL FOR 1600N SURVEY LINE

Line 1600N indicates the presence of the high resistivity earth materials beneath survey line except for very locally limited low resistivity material on the top most middle zones between -560m and -320m on x-location. An extremely high resistivity materials exist on east of inverse model with almost all homogeneous geological material. This homogeneous high resistivity material invaded the country rocks and form horizontal to vertical penetrative contact. The depth extension of an intrusion does not known from this inverted model. However the lateral extension is limited within survey line, regardless of a dyke emanate from a source and an alteration of the country rocks that extended beyond lateral limitation of a survey line.

An intrusive body shows low chargeability (figure 5.23) which slightly varied down ward, while chargeability increases as far as move away from an intrusion on both side, but high chargeability material is located at the left top most layer localized between -780m and -560m. Chargeability decreases with the depth on both left and right side of an intrusive body.

Generally, line 1600N inverted pseudo section shows that resistivity and chargeability of the subsurface materials through the depth has an inverse proportionality.

As evidenced from drill hole log (DH1650N/2) located at 474979E and 566190N near 1600N survey line in vicinity of -570m on horizontal distance, the inverted section reveals existence of chlorite actinolite schist and carbonate chlorite schist intruded by mineralized metagranodiorite. Metagranodiorite exist as an intrusive body confined in small circular area between -620m and -560m around 45m depth with high resistivity and chargeability anomaly. High resistivity and low chargeability on the right portion of inverted model is plutonic body which is concisely correlated to metagabbro/amphibolite.

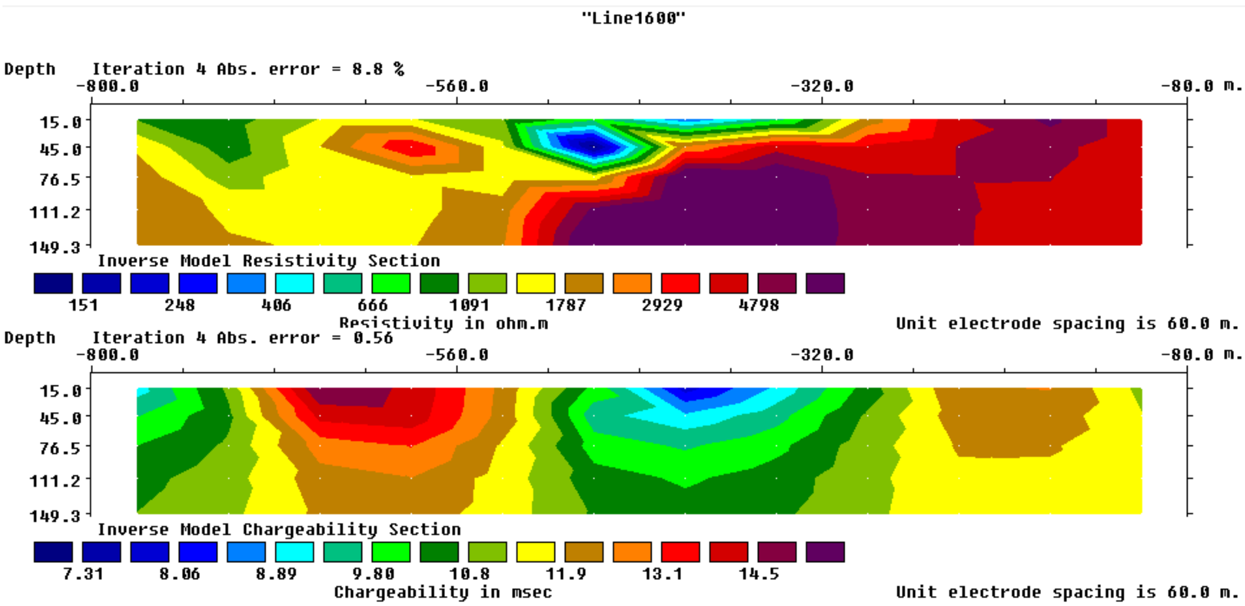

Figure 5.23. Inverse model of resistivity and chargeability for line 1600N

5.4.8. RESISTIVITY AND CHARGEABILITY INVERSE MODEL FOR 1700N SURVEY LINE

The following resistivity and chargeability inverse models reveal subsurface variation of the rock material's physical properties beneath 1700N survey line.

Resistivity inverse model display three section among which two of them show high resistivity and one low resistivity section. High resistivity zones from 3000Ωm to 5000Ωm are situated on large area and it is interpreted as an intrusive body.

A series of faults area clearly visible on both side termination of an intrusion and High resistivity materials are followed the nearly vertical contacts portrayed on right side of the intrusion. However low resistivity materials that show the series of thin layers are overlay the entire high resistivity and the layers are offset along a fault zone. These tectonically unstable stratified top layers are interpreted as meta-sediment (schist).

Chargeability inverse model (figure 5.24) comprises two major left and right sections. The left section is intermediate chargeability section. It hosts locally limited high chargeability anomalies at -480m to -530m on the horizontal distance with 45m depth. The right section consists of high chargeability whose values increase left to right starting from an intrusion. High chargeability material (>14msec) is located at -260m to 140m on x- location within the shallow depth up to 60m.

Based on drill hole log (DH1700N/3) located at 475081E and 566209N in vicinity of -480m on horizontal distance, the top layers of relatively low resistivity (<2300Ωm) and (2300Ωm-3500Ωm) are correlated to carbonate chlorite schist and meta-granodiorite respectively, whereas high resistivity anomaly (>3500Ωm) massive intrusive body is correlated to metagabbro/amphibolite. Carbonate chlorite schist indicates horizontal layering which confirm existence of sedimentary rocks or sedimentary rocks origin.

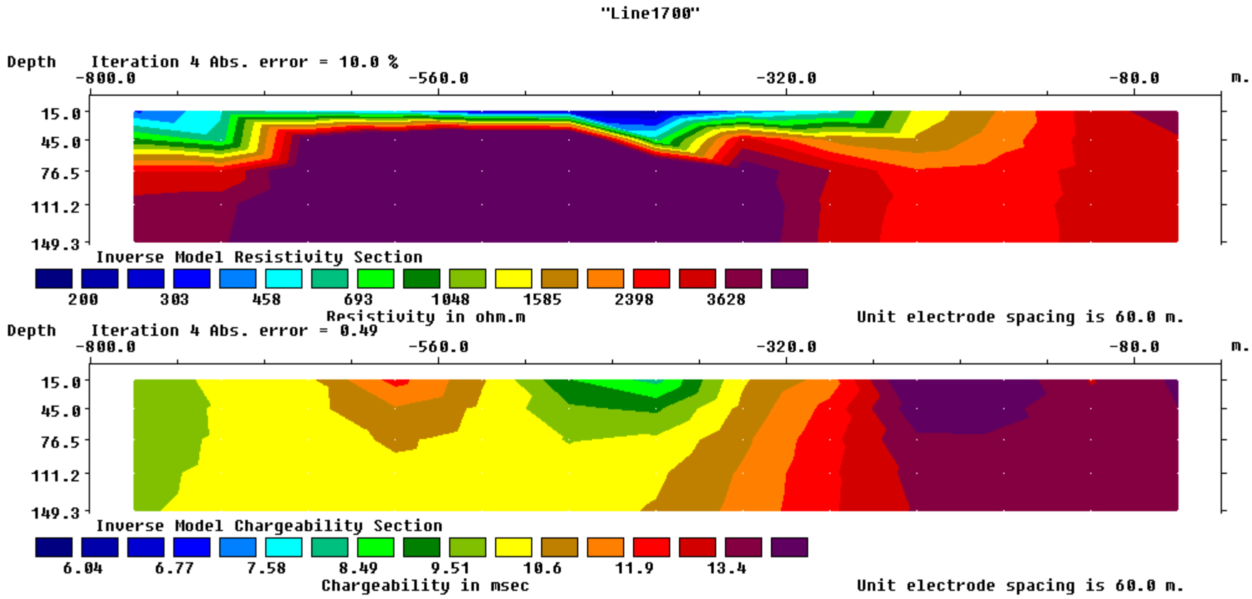

Figure 5.24. Inverse model of resistivity and chargeability for line 1700N

CHAPTER SIX

6. CONCLUSION AND RECOMMENDATION

6.1. CONCLUSION

Based on integrated geophysical and drill hole log data, lithologies of the project area are concluded into the following three main rocks.

1) Schist: this lithology covers large lateral extent and depth of the study area and hosts carbonate chlorite schist and chlorite actinolite schist. It shows relatively low to intermediate resistivity and locally high chargeability anomalies.
2) Metagranodiorite: metagranodiorite exists as an intrusion and reveals high resistivity and high chargeability anomalies. It covers small area on west part of study area and in little eastern zones of surveyed area.
3) Metagabbro: These zones are huge massive intrusive bodies located at southern and northern part of study area showing high resistivity and low chargeability.

Generally, high chargeability anomalies are dominantly indicated within schists and metagranodiorite on two middle survey lines along 1150N and 1400N. Resistivity and chargeability plan maps depict that, sulphides mineralization increases with depth as it able to be interpreted from n-spaces (n_1, n_2, n_4 and n_6) plan maps.

N1, N2 and N4-level chargeability plan maps indicate lateral continuity of the high chargeability anomalies body in Northwest direction, whereas N-6-level chargeability plan map reveals continuity of the mineralization in the South and Southwest direction.

Generally, lack of good correlation of geophysical and drill hole log data that discussed and recommended by the previous researchers were solved. There is concise correlation of geophysical and drill hole log data, however there are a numbers of the dykes which are interpreted as the layers by drill hole interpreters.

Magnetic survey had been done to enhance resistivity and induced polarization data through identifying structures and magnetically anomaly zones of area. East, Southwest, Northwest, Northeast and central zones are dominantly host high magnetic anomaly with geological structures and features trending in to three directions.

6.2. RECOMMENDATION

N1, N2 and N4-level chargeability plan maps indicate lateral continuity of the high chargeability anomaly bodies in Northwest direction, whereas N-6-level chargeability plan map reveals continuity of mineralization in the South and Southwest directions. In order to include all suggested laterally opened chargeability anomalies in to plan maps and inverse models, extending of the survey line on west side to the sites of above mentioned laterally opened high chargeability anomalies area are strongly recommended for the further studies.

Inverse chargeability models along the survey lines (1150N and 1400N) and N6-level plan map depict an open high chargeability anomalies to the depth as indicated on the maps. These continuities of high chargeability anomaly with the depth need further studies by increasing n-spacing on the same unit electrode spacing (a=60m).

Res2dinv is computer programming software used to plot 2D inverse maps. The four iteration number software was used to display inverse model for both resistivity and chargeability gridded data acquired from all dipole- dipole array survey lines. However, it is recommended if inversion soft wares of the greater iteration number is used to get the more fit calculated resistivity pseudo sections and measured resistivity pseudo sections than that of compiled in this thesis report.

Reconnaissance survey of gradient array was applied on the 950N and 1050N survey lines show high resistivity and high chargeability at the west of zone confined between lines. In order to get true depth and inverse model of this anomaly body, it needs detail study by using dipole-dipole array.

Magnetic survey indicates the presence of magnetic minerals in the area. The data are collected by 40m spacing along each survey lines. However it is recommended to use 20m observation spacing to get more detail delineated magnetic nature in the area

REFERANCES

1) Abera Alemu. (2020). Principles, Practices and Applications of Geophysical methods to resource Exploration and Geohazard studies. Aster Naga Publishing Enterprise, Addis Ababa, Ethiopia, 560pp.
2) Abu Wube. (2005). Minerelization and associated structures of Okote Prospect. Addis Ababa. Ethiopia, 11pp.
3) A. Asrat, Barbery and G. Gliezes. (2001). Precambrian Geology of Ethiopia: a review. African geoscience review. 8:271 – 288.
4) A.Y.Billay, A.F.M. Kister, A.F. Mayer, J. Schalider.(1997).Geology of lega Dembi gold deposit, southern Ethiopia. Implication for pan African gold exploration.32:491-504.
5) Alan,E.(2000). Look into the Earth: an introduction to the Geological Geophysics. Cambridge University press, New york, 493pp
6) Behailu Mammo. (2015). Integrated analysis and interpretation of Helicopter borne aeromagnetic and Gamma ray spectrometric data of South Maleka (Adola Green stone Belt). Addis Ababa. Ethiopia, 79pp.
7) C.D.Gribble.(1988).Rutley's element of mineralogy,2nd edition.
8) Debele.J.D and Koeberl.C.(2004).geochemistiry alteration and genesis of gold mineralization in Okote area, Southern Ethiopia. Geochemical journal.38:307-331.
9) Deksisa Debele.(1993).The geology and mineralization and geochemical exploration of Adola-Aflata area.Southern Ethiopia.
10) Dr.M.H.Loke.(2012).2-D and 3-D electrical imaging survey. 172pps
11) Ethiopia institute of Geological Survey (1996). Explanation of the geological map of Ethiopia, second edition, Addis Ababa, Ethiopia, 85pps
12) Ethiopia institute of Geological Survey (1994). Geology of agree Mariam, Addis Ababa, Ethiopia, 122pps
13) Ethiopia institute of Geological Survey (1998). Geology of Nagelle area, unpublished technical report, Addis Ababa, Ethiopia, 141pps
14) Ethiopia institute of Geological Survey (1989). Geophysical investigation for primary gold in okote area, unpublished technical report, Addis Ababa, Ethiopia, 16pps

15) Ethiopia institute of Geological Survey (1997). Induced polarization and resistivity survey in Okote area, unpublished technical report, Addis Ababa, Ethiopia, 29pps

16) Ethiopia institute of Geological Survey (1991). Gravity survey on selected profiles across the Adola Belt , unpublished technical report, Addis Ababa, Ethiopia, 27pps

17) Geological survey of Ethiopia (2007).Magnetic and spectral induced polarization (SIP)/resistivity signatures of Buri-karo prospected, Adola Belt, Addis Ababa, Ethiopia, 64 pps.

18) Geological survey of Ethiopia (2003). Industrial Minerals and Rocks resource potential of Ethiopia, Addis Ababa, Ethiopia, 77pps.

19) Geological survey of Israel Ministry of development (1963). Geology of Ethiopia, unpublished technical report, Addis Ababa, Ethiopia.

20) Geological survey, UNDP project (1993). Final report on mineral exploration in Adola area, Addis Ababa, Ethiopia

21) Geological survey of Ethiopia, ministry of mines and energy (2006).Final report on Induced polarization and resistivity survey in okote area, Addis Ababa, Ethiopia, 43pp.

22) Girma Woldetinsae, Mersha Nigussie, Yiheyis Kebede, H/Selassie, G/Silassie.(1997). Induced polarization and resistivity survey in Okote area. Adola district.Southern Ethiopia.

23) Jenbere Shiferaw.(1989).Geophysical investigation for primary gold in Okote area.southern Ethiopia.

24) John, M. (2003). Field Geophysics, third edition.John Wiley and sons Ltd, England, 249pps.

25) Mark, E. (2013). Near surface applied geophysics. Cambridge University press, New York, 442pps.

26) Michael, B. (2002). An introduction to the Geophysical exploration, third edition. Blackwell Science Ltd, 281pp.

27) Robert,J. (1999). Whole Earth Geophysics: An introductory text book for Geologist and Geophysist. Simon and Schuster/ a Viacom company, United State of America, 192pp.

28) Solomon Gada.(2015).Geochemistry, alteration and genesis of granodiorite hosted gold mineralization in okote area.Addis Ababa University. Ethiopia, 118pp.

29) Solomon Gada.(2019).The role of intrusion in orogenic polyphase gold mineralization, okote area. Addis Ababa Science and Technology University. Ethiopia, 74pp

30) William, L. (2007). Fundamental of Geophysics, second edition. Cambridge University press, New York, 393pp.